Cleft lip and cleft palate (CL/P) in *Esrp1* KO mice is associated with alterations in epithelial-mesenchymal crosstalk

SungKyoung Lee[1*], Matthew J. Sears[1], Zijun Zhang[3,4], Hong Li[5], Imad Salhab[6], Philippe Krebs[7], Yi Xing[3,4], Hyun-Duck Nah[6], Trevor Williams[5], and Russ P. Carstens[1, 2*]

Departments of Medicine[1] and Genetics[2], Perelman School of Medicine, University of Pennsylvania, Philadelphia, Pennsylvania, 19104, USA

Center for Computational and Genomic Medicine, The Children's Hospital of Philadelphia[3], Philadelphia, Pennsylvania, 19104, USA

Department of Pathology and Laboratory Medicine, Perelman School of Medicine, University of Pennsylvania, Philadelphia, Pennsylvania, 19104, USA[4]

Department of Craniofacial Biology[5], University of Colorado School of Dental Medicine, Aurora, CO 80045, USA

Division of Plastic and Reconstructive Surgery, The Children's Hospital of Philadelphia[6], Philadelphia, Pennsylvania, 19104, USA

Institute of Pathology[7], University of Bern, Bern Switzerland

KEYWORDS: Cleft lip; cleft palate; epithelial-mesenchymal crosstalk; lip morphogenesis

Author for correspondence: russcars@upenn.edu

SUMMARY STATEMENT

Ablation of the epithelial-specific splicing factor *Esrp1* leads to cleft lip and cleft palate (CL/P) and this study identifies alterations in Wnt signaling during face formation that may partly underlie this defect.

ABSTRACT

Cleft lip is one of the most common human birth defects. However, there remain a limited number of mouse models of cleft lip that can be leveraged to characterize genes and mechanisms that cause this disorder. While crosstalk between epithelial and mesenchymal cells underlies formation of the face and palate, the basic molecular events mediating this crosstalk remain poorly understood. We previously demonstrated that mice lacking epithelial-specific splicing factor *Esrp1* have fully penetrant bilateral CL/P. In this study we further investigated the mechanisms leading to cleft lip as well as cleft palate in both existing and new *Esrp1* mutant mouse models. These studies included a detailed transcriptomic analysis of changes in ectoderm and mesenchyme in *Esrp1*$^{-/-}$ embryos during face formation. We identified altered expression of genes previously implicated in cleft lip and/or palate, including components of multiple signaling pathways. These findings provide the foundation for detailed investigations using *Esrp1* mutant disease models to examine gene regulatory networks and pathways that are essential for normal face and palate development and whose disruption leads to orofacial clefting in human patients.

INTRODUCTION

Cleft lip with or without cleft palate (CL/P) and cleft palate only (CP or CPO) are among the most common congenital birth defects, affecting approximately 1 in 700 live births and affected children face a variety of health and psychosocial problems as well as a need for extensive surgical and dental treatments (Dixon et al., 2011). The causes of CL/P and CP are heterogeneous and include both environmental and genetic factors. Although either CL/P or CP can be a component of disease syndromes, most cases are non-syndromic. Cleft lip with or without cleft palate (CL/P) is more common in human patients than isolated cleft palate (CP) and these disorders are largely genetically and etiologically distinct (Fraser, 1970; Gritli-Linde, 2008). The proper development of the lip and palate is similar between humans and mice and thus mouse models have served an important role in studies to identify genes and characterize pathways that, when disrupted, lead to CL/P or CP (Gritli-Linde, 2012; Juriloff and Harris, 2008). In mice, formation of the face commences around E9.5 and involves the five facial prominences consisting of mostly neural crest-derived mesenchyme and overlying epithelium; the frontonasal prominence (FNP) and the paired maxillary and mandibular prominences (MXP and MdP) (Jiang et al., 2006). The FNP gives rise to the lateral and medial nasal prominences (LNP and MNP) and these prominences grow into close apposition and by E12.5 the nasal and maxillary prominences fuse to form the upper lip and primary palate. Defects in the growth and/or fusion of these prominences result in CL/P. The formation of the secondary palate is a separate developmental process that occurs from E12-E15.5 when the palatal shelves emerge from the maxillary prominences, elevate, and fuse in the midline (Jiang et al., 2006). Defects in any of these steps can lead to cleft palate (CP). While CL/P is the more common human clinical presentation, there are many mouse models of CP, yet relatively few for CL/P (Gritli-Linde, 2008). Thus, newer mouse models for CL/P are needed to further define genes and pathways involved in CL/P pathogenesis. During craniofacial development, the epithelial cells of the facial prominences and palate provide signals required for mesenchymal proliferation and patterning. At the same time the mesenchyme provides feedback to epithelial cells and these reciprocal epithelial-mesenchymal interactions are crucial for normal facial and palatal development (Jiang et al., 2006; Wedden, 1987). These interactions involve signaling pathways for the Wnt, TGF-β/Bmp, Hedgehog, and Fgf families and mutations in components of these signaling pathways have been shown to cause CL/P and CP in human patients (Reynolds et al., 2019).

We identified the Epithelial Splicing Regulatory Proteins 1 and 2 (ESRP1 and ESRP2) as epithelial-specific regulators of multiple target transcripts, including an event in fibroblast growth factor receptor 2 (Fgfr2) whose dysregulated splicing is associated with cleft palate (Bebee et al., 2015; Rice et al., 2004; Warzecha et al., 2009a). While there is some functional redundancy between these two paralogous proteins, only ESRP1 is essential, since loss of ESRP2 alone does not overtly alter splicing and *Esrp2* KO mice have no apparent phenotype (Bebee et al., 2015; Warzecha et al.,

2009b). In contrast, the loss of ESRP1 alone can lead to substantial alterations in splicing of numerous target transcripts, albeit the loss of both ESRP1 and ESRP2 is associated with larger changes in splicing. We previously showed that ablation of *Esrp1* alone in mice led to fully penetrant bilateral CL/P, adding this splicing factor to the limited number of genes whose ablation leads to this defect in mice (Bebee et al., 2015). We therefore hypothesized that facial development is dependent on ESRP1-regulated splicing events and that studies using these mice have the potential to reveal novel molecular mechanisms whose dysregulation leads to CL/P. We carried out a detailed analysis of the defects in facial and palatal development and an extensive analysis of changes in alternative splicing in the epithelial cells of the facial prominences - as well as changes in total gene expression - in both epithelial cells and underlying mesenchyme. We identified reduced expression of several genes in *Esrp1* KO ectoderm, including several canonical Wnts, as well as sonic hedgehog (Shh). These gene expression changes were accompanied by reduced expression of canonical Wnt target genes, transcriptional targets of Shh signaling, and components of the TGF-β/Bmp pathway in adjacent mesenchyme. These observations indicate that ESRP1 plays an important role in epithelial-mesenchymal cross-talk during craniofacial development. We also noted a defect in epithelial cell fusion during lip formation and in palatal explant cultures indicating that ESRP1 is required for two distinct processes, growth and fusion, that are required for proper lip and palatal formation.

RESULTS

Condition ablation of *Esrp1* in surface ectoderm leads to CL/P

We examined the tissue specificity of ESRP1 in the developing face and palate by generating mice with endogenously FLAG epitope tagged ESRP1. Analysis of these mice (*Esrp1*$^{FLAG/FLAG}$ mice, Fig. S1) confirmed that ESRP1 protein is specifically expressed in surface ectoderm at E11.5 as well as epithelial cells of the secondary palate as previously shown for *Esrp1* mRNA (Revil and Jerome-Majewska, 2013; Warzecha et al., 2009a). We generated mice with conditional ablation of *Esrp1* in surface ectoderm derived from *Esrp1*$^{flox/flox}$ mice and transgenic *Crect* mice that express Cre specifically in surface ectoderm and derivatives starting at E8.5, a time point prior to lip fusion (Reid et al., 2011). We confirmed relatively efficient conditional ablation in epidermis of *Esrp1*$^{flox/flox}$*; Crect*$^{+/-}$ E18.5 embryos (Fig. S2). Compared to littermate controls, we noted bilateral CL/P in *Esrp1*$^{flox/flox}$*; Crect*$^{+/-}$embryos at E18.5 (Fig. 1A). While the phenotype was less extensive than previously observed in *Esrp1*$^{-/-}$ mice, there was a clear cleft of the primary palate and failure of the lip processes to come together to form a midline philtrum. We also performed staining for bone and cartilage structures which confirmed a completely cleft secondary palate and a bilateral cleft of the

primary palate. The palatine bones (p) were hypoplastic and located to the side and the palatal processes of the maxilla (ppmx) were similarly dysmorphic. The premaxilla (pm) was undeveloped with a poor connection to the maxilla (m) and thus extended out in front of the face. (Fig. 1B).

In contrast to mice with complete ablation of *Esrp1*, mice with an ENU-induced point mutation in a highly conserved region of *Esrp1* (*Esrp1*$^{Triaka/Triaka}$ mice) had modestly altered intestinal function, but no craniofacial defects (Mager et al., 2017). Whereas neither *Esrp1*$^{+/-}$ mice, nor *Esrp1*$^{Triaka/Triaka}$ homozygous animals showed overt craniofacial defects, the faces of compound mutant *Esrp1*$^{triaka/-}$ pups (5 /5), while showing some hypoplasia compared to littermate controls, had clefting of the secondary soft and hard palate, but no apparent cleft of the lip or primary palate (Fig 1C). These data show that this null/hypomorph allelic combination is able to generate a model of cleft secondary palate in the absence of cleft primary palate, indicating that these two developmental processes are not linked, but have different sensitivities to the levels of active ESRP1. The observation of a cleft secondary palate in the absence of cleft lip in *Esrp1*$^{Triaka/-}$ pups strongly indicated that *Esrp1* deficiency independently leads to a failure in palate formation.

Esrp1 ablation leads to reduced outgrowth of facial prominences associated with reduced epithelial and mesenchymal cell proliferation.

Lip formation results from outgrowth and fusion of the MxP, LNP, and MNP and failure in either process can lead to cleft lip. Ki67 staining of MNP and LNP in sections from E10.5 embryos showed reduced cell proliferation in both epithelial and mesenchymal cells associated with less apparent growth of the two processes towards apposition (Fig. 2A). Evaluation of apoptosis using staining for activated caspase 3 showed no apparent differences between control and knockout embryos other than the expected apoptosis in sections where these MNP and LNP processes were beginning to fuse in control embryos. In *Esrp1*$^{-/-}$ mice these processes either did not make contact, or if they did make contact there was no observed fusion and no apparent apoptosis at the sites of contact (Fig. 2B). In one case where we observed contact between the MNP and LNP in *Esrp1*$^{-/-}$ mice, we noted that there was persistent expression of E-Cadherin that was not observed in wild-type (WT) embryos (Fig 2C). We conclude that a reduction in proliferation of facial prominences contributes to CL/P in *Esrp1*$^{-/-}$ mice, but that there is also a defect in fusion when these processes make contact. Nonetheless, the reduction in cell proliferation in mesenchyme adjacent to *Esrp1* ablated epithelial cells indicated that there was a disruption in a communication pathway from epithelium to mesenchyme during facial development.

We used scanning electron microscopy (SEM) to further evaluate lip formation and fusion in WT and *Esrp1*$^{-/-}$ embryos at different stages of lip formation. At E10.5, WT embryos showed the onset of fusion between the MNP and LNP, LNP and MxP, and MNP and MxP at the 3-way lambdoid

junction. At E11.5 the fusion between these processes was more complete and by E12.5 there was normal development of the upper lip and nasal pit (Fig. 2D). In *Esrp1*$^{-/-}$ embryos the LNP and MNP were smaller and there remained a gap between them that resulted in a larger nasal pit (Fig. 2D). Compared to WT embryos, the MNP and LNP were further separated from each other, but in some cases there was contact between these processes, but no apparent fusion. There was also no contact observed between the hypoplastic MxP and either MNP or LNP to generate a typical lambdoid junction. By E12.5 there was very little contact noted between any of the prominences other than one example where there was some contact between MNP and LNP deeper into the nasal pit. Taken together, the SEM studies showed that while there was some reduction in size of the facial prominences, there were some cases where contact occurred between MNP and LNP, but this was not followed by fusion. These observations, together with sections of these prominences in E10.5 embryos, further indicated that reduced proliferation and a defect in fusion underlie the CL/P phenotype.

Palatal processes show reduced proliferation as well as a defect in fusion during palatogenesis. The studies using SEM and histology suggested that CL/P in *Esrp1*$^{-/-}$ mice was due to both a defect in fusion and in cell proliferation. We also noted reduced outgrowth of the palatal shelves towards each other, suggesting that they also likely had a defect in cell proliferation. Analysis of secondary palate formation in *Esrp1*$^{-/-}$ E16.5 embryos using Ki67 staining and cleaved caspase 3 detection confirmed that the palatal shelves had a proliferation defect without apparent differences in apoptosis compared to wild-type embryos (Fig 3A). However, because the palatal shelves did not make contact *in vivo* in *Esrp1*$^{-/-}$ mice, we were unable to directly determine whether there was an associated fusion defect. Therefore, to further evaluate the defect in palatogenesis in *Esrp1*$^{-/-}$ mice we performed palatal organ culture assays. WT and *Esrp1*$^{-/-}$ palatal shelves were isolated from E13.5 embryos and cultured for up to 72 hours. Palatal shelves from WT embryos grew together within 48 hours and after adhering underwent fusion with dissolution of the medial epithelial seam (MES) and mesenchymal confluence (N=7/7). Evaluation of palatal cultures from *Esrp1*$^{-/-}$ mice was complicated by increased fragility and reduced proliferation such that contact between opposing palatal shelves was delayed. Nonetheless, we noted that while the palatal shelves from eight out of thirteen *Esrp1*$^{-/-}$ embryos were able to achieve contact, in seven of the eight palatal cultures where the palatal processes achieved adherence there was no dissolution of the medial edge epithelial cells and a failure to achieve mesenchymal confluence. Only one of the eight *Esrp1*$^{-/-}$ palatal shelves that made contact showed partial dissolution of the MES and a small region of apparent mesenchymal connection. For one representative control and one *Esrp1*$^{-/-}$ sample in which the palatal processes made contact, we performed staining for the epithelial marker E-cadherin as well as activated caspase 3 and Ki67. In the wild-type cultures, we

observed a nearly complete loss of E-cadherin expression in cells at the site of fusion as well as the expected apoptosis at the fusion site. However, in the *Esrp1*$^{-/-}$ palates that achieved close contact, there was persistence of the MES and an absence of mesenchymal confluence (Fig. 3B, additional examples in Fig. S3). These results demonstrate that while reduced growth and proliferation of palatal shelves contribute to the cleft palate defect, there is also a defect in fusion and dissolution of the MES. The results from the palatal explant cultures also further verify that the clefting of the secondary palate in *Esrp1*$^{-/-}$ mice represents an independent defect.

Ablation of Esrp1 leads to large scale changes in splicing in surface ectoderm.

The specific expression of ESRP1 in surface ectoderm together with the CL/P defect observed in *Esrp1*$^{flox/flox}$*;Crect*$^{+/-}$ embryos indicated that alterations in the transcriptome of surface ectoderm derived cells underlie orofacial clefting in *Esrp1*$^{-/-}$ mice. However, the reduction in cell proliferation observed in the mesenchyme adjacent to epithelial cells also indicated that gene expression alterations in *Esrp1*$^{-/-}$ epithelial cells induced changes in signaling crosstalk from epithelium to mesenchyme. To further investigate the molecular mechanisms that lead to CL/P in *Esrp1*$^{-/-}$ mice, we performed RNA-Seq using RNAs collected from both epithelial cells and mesenchymal cells from control and *Esrp1*$^{-/-}$ embryos. We used a previously described method to separate facial ectoderm and mesenchyme from facial prominences at E12.0, a stage at which lip fusion is underway (Li and Williams, 2013). We prepared RNA from four replicate samples each of ectoderm and mesenchyme in WT and *Esrp1*$^{-/-}$ embryos and performed RNA-Seq. We used paired end sequencing and obtained an average of 100 million read pairs per replicate. Preliminary analysis of RNA-Seq reads from epithelial and mesenchymal control samples validated that they were derived from relatively pure populations of each cell type using a panel of standard epithelial and mesenchymal cell type-specific markers, including *Esrp1* (Fig. 4A). To identify genome-wide alterations in splicing in ectoderm from *Esrp1* KO embryos compared to WT controls we used replicate-based multivariate analysis of transcript splicing (rMATS)(Shen et al., 2014). We also used rMATS to identify global differences in splicing of epithelial cells compared to mesenchymal samples using RNAs from control embryos. In *Esrp1* KO epithelial cells rMATS identified a total of 1467 alternative splicing changes compared to wild-type (WT) epithelial cells, with cassette exons (skipped exons (SE)) representing the largest fraction (Fig.4B, 4C, Table S1). Analysis of splicing differences between WT epithelial cells and WT mesenchymal cells identified 2546 splicing events, including many Esrp-regulated events that switch splicing from epithelial to mesenchymal splice variants after *Esrp1* ablation (Fig. 4B, 4D, Table S2). The larger number of splicing differences between epithelial and mesenchymal cells compared to *Esrp1*$^{-/-}$ epithelial cells is consistent with previous studies by our group and other investigators showing combinatorial regulation of splicing events that are induced during EMT or that differ between epithelial and mesenchymal cells by several splicing factors, including ESRP1/2, but also other splicing regulators (Braeutigam et al., 2014; Pillman et al., 2018; Shapiro et al., 2011; Venables

et al., 2013; Yang et al., 2016). We validated 19 cassette exon (SE) events in WT compared to *Esrp1*$^{-/-}$ ectoderm with the most highly statistical significance and largest absolute change in Percent Spliced In (PSI) by semi-quantitative RT-PCR (Figure 4E; Table S1). We also validated 6 representative examples of splicing differences between control ectoderm and control mesenchyme (Fig. 4F). As expected, a change in alternative splicing of *Fgfr2* was identified among alterations in mutually exclusive (MXE) exon splicing in *Esrp1*$^{-/-}$ ectoderm. This event involves two alternative exons, named IIIb or IIIc, that encode a region in the extracellular ligand binding domain and with the resulting receptor isoforms, FGFR2-IIIb and FGFR2-IIIc, having different FGF binding preferences (Zhang et al., 2006). We confirmed this splicing switch by RT-PCR, which showed a switch from nearly complete splicing of the epithelial-specific IIIb exon to predominant splicing of the mesenchymal IIIc exon in *Esrp1*$^{-/-}$ ectoderm (Fig. 4E). Both global splicing comparisons were subjected to Gene Ontology analysis and revealed overlapping enrichment terms for both splicing comparisons, including cytoskeletal organization, cell morphogenesis, and cellular component organization (Fig. 4G, H). Similarly, Kyoto Encyclopedia of Genes and Genomes (KEGG) pathway analysis demonstrated an enrichment for terms including adherens junctions, suggesting that alternatively spliced genes contributed to epithelial functions (Fig. 4G, H). KEGG analysis in WT compared to *Esrp1*$^{-/-}$ ectoderm also showed enrichment for components of the Hippo pathway, which has been implicated in human clefting disorders (Williamson et al., 2014).

Ablation of *Esrp1* in ectoderm is associated with altered expression of genes associated with cleft lip and/or palate and disruptions in signaling crosstalk in underlying mesenchyme. We also investigated changes in total transcript levels in *Esrp1* ablated epithelial cells, as well as in adjacent mesenchyme. In epithelial cells we identified 167 downregulated genes and 546 upregulated genes (Table S3). Among the downregulated genes we noted six transcripts encoding canonical Wnt ligands, Wnt3, Wnt3a, Wnt4, Wnt7b, Wnt9b, and Wnt10b, each of which were downregulated approximately 2-fold, of which several were validated by RT-qPCR (Fig. 5A). We also noted downregulation of Wls, which is required for Wnt secretion. Consistent with these observations, for genes downregulated in *Esrp1* KO ectoderm, Wnt signaling pathway was an enriched gene ontology (GO) term for biological process and was also enriched by KEGG pathway analysis (Fig. 5B). We also noted an increase in both *Aldh1a2* and *Aldh1a3*, which generate retinoic acid and have been implicated in feedback regulation of Wnt signaling during craniofacial development (Osei-Sarfo and Gudas, 2014; Song et al., 2009). We examined whether the downregulation of Wnt ligands in the ectoderm was also associated with a corresponding reduction in targets of canonical Wnt/beta-catenin signaling in mesenchyme as previously shown in *Wnt9b* and *Lrp6* KO mice with CL/P (Jin et al., 2012). Interestingly, we identified larger changes in gene expression in mesenchyme of *Esrp1*$^{-/-}$ mice than in ectoderm, with 3048 upregulated genes and 2396 downregulated genes (Table S3). In addition we also identified genes that were differentially expressed in wild-type ectoderm compared to wild-type mesenchyme, which included numerous known epithelial and mesenchymal markers (Table S5).

While Wnt signaling was not among the most enriched GO terms or pathways for genes downregulated in *Esrp1*$^{-/-}$ mesenchyme compared to wild-type mesenchyme, we noted numerous canonical Wnt targets among downregulated genes under the "Wnt signaling pathway" category, several of which were also validated by RT-qPCR along with several other genes encoding components of the Wnt pathway (Fig. 5A). We also noted reduced expression of Sonic hedgehog (Shh) in *Esrp1*$^{-/-}$ ectoderm and a corresponding reduction in expression of the *Gli1*, *Gli2* and *Gli3* transcription factors in mesenchyme, with the greatest reduction in *Gli2* confirmed by RT-qPCR (Fig. 5A). We also identified several other genes with reduced expression in *Esrp1*$^{-/-}$ mesenchyme that have previously been implicated in cleft palate, including *Bmp7*, *Tgfb2*, and *Tgfb3* (Fig. 5A, Table S4) (Kaartinen et al., 1995; Kouskoura et al., 2013; Proetzel et al., 1995; Sanford et al., 1997). Thus, we identified transcriptomic in multiple signaling pathways including several that have previously been shown to play an essential role in lip/palate morphogenesis (Table S6). We validated reduced expression of *Wnt9b* and *Shh* in *Esrp1*$^{-/-}$ mice using in situ hybridization (ISH) in mouse embryos at E10.5-11.5. The reductions in these transcripts were limited to facial ectoderm in *Esrp1*$^{-/-}$ embryos, consistent with the RNA-Seq data showing that *Wnt9b* and *Shh* were specifically expressed in ectoderm (Fig. 5C, Table S3). We also confirmed reduced expression of canonical Wnt targets *Lef1* and *Axin2* using both whole mount and section ISH (Fig. 5D).

To further examine canonical Wnt signaling during facial development in *Esrp1*$^{-/-}$ mice, we crossed both WT and *Esrp1*$^{-/-}$ mice with *TCF/Lef:H2B-GFP* transgenic reporter mice that express an H2B-EGFP fusion protein under the control of six copies of the TCF/LEF response element (Ferrer-Vaquer et al., 2010). In *Esrp1*$^{-/-}$ E11.5 embryos we noted reduced reporter activity in both the ectoderm and mesenchyme of the NPs and MxP, although the reduction in mesenchyme was more pronounced in MxP than the MNP or LNP (Fig. 6A). Because of some differences in various Wnt reporter models and to further verify changes in canonical Wnt signaling, we also used *Axin2*^{lacZ} mice in which LacZ is knocked in at the endogenous *Axin2* locus as a second readout for Wnt signaling in WT vs. *Esrp1*$^{-/-}$ embryos. At E10.5 we noted that although there was no apparent difference in LacZ expression in the LNP, there was pronounced reduction in LacZ in both the ectoderm and mesenchyme of the MNP (Fig. 6B). We also noted reduced LacZ in the MxP at E11.5. Taken together, these observations are consistent with the results from RNA-Seq showing reduced Wnt expression in ectoderm of *Esrp1*$^{-/-}$ embryos and an associated reduction in canonical Wnt targets. These findings are consistent with a model in which *Esrp1* ablation leads to alterations in in epithelial-mesenchymal interactions that underlie normal face facial development.

DISCUSSION

Studies using mouse models have played a major role in our understanding of the morphogenetic programs in the face and palate that, when disrupted, lead to cleft lip and/or without cleft palate. Mouse models have been particularly informative in defining genes and pathways whose disruption leads to cleft palate only (CPO) (Li et al., 2017). However, there remain relatively few mouse models that lead to CL/P, such as those involving mutations or deletions of *Wnt9b*, *Lrp6*, *Bmp4*, *Bmpr1a*, *Tfap2a*, and *Pbx1/2* (Ferretti et al., 2011; Green et al., 2015; Gritli-Linde, 2012; Jin et al., 2012; Juriloff and Harris, 2008; Juriloff et al., 2006; Liu et al., 2005; Song et al., 2009). As a result, our understanding of molecular mechanisms involved in the formation of the lip and primary palate have lagged behind those described for formation of the secondary palate. Our identification of fully penetrant CL/P in *Esrp1*$^{-/-}$ mice provides a new genetic model that can be exploited to further investigate mechanisms of lip development. It is notable that while much has been learned about signaling and transcription factors that are involved in craniofacial development, the role of alternative splicing in lip and/or palate development has been largely unexplored. Prior to our identification of CL/P in *Esrp1* KO mice, no studies have identified roles of splicing factors in CL/P. Furthermore, other than the role of a specific splice variant for *Fgfr2* (Fgfr2-IIIb), the possibility that the functions of some genes required for face and palate development are splice isoform-specific has not generally been considered. There is now firm evidence that, like transcription factors, tissue-specific splicing regulators coordinate programs of AS involving transcripts that encode proteins that function in biologically coherent pathways (Kalsotra and Cooper, 2011; Lee et al., 2018; Ule et al., 2005; Zhang et al., 2008). Thus, our studies demonstrating that *Esrp1* is required for formation of both the lip and palate indicates that gene targets of ESRP1 regulation also play essential developmental roles and that mutations in these genes may cause or predispose patients to CL/P.

Our finding of bilateral CL/P in *Esrp1*$^{flox/flox}$*;Crect*$^{+/-}$ embryos indicated that ablation of *Esrp1* in early surface ectoderm and derivatives underlies cleft lip and cleft palate. Therefore, identification of transcriptomic changes in this cell population is key to understanding mechanisms leading to this defect. We considered the possibility that the cleft palate observed in *Esrp1*$^{-/-}$ and *Esrp1*$^{flox/flox}$*;Crect*$^{+/-}$ mice embryos might be a consequence of cleft primary palate extending into the secondary palate. However, mice with compound ablation of *Esrp1* and a hypomorphic *Esrp1 Triaka* allele (*Esrp1*$^{Triaka/-}$ mice) had no cleft lip or primary palate but a cleft secondary palate, indicating that *Esrp1* is independently required for secondary palate (Mager et al., 2017)(Fig. 1D). These studies establish that ESRP1 is required for both lip and palate development and that both *Esrp1* mutant models can be used to characterize mechanisms that are essential for both developmental processes.

We examined proliferation using Ki67 staining and identified reduced staining in epithelial and mesenchymal cells of the MNP and LNP. There was also reduced Ki67 staining in the palatal shelves of *Esrp1*$^{-/-}$ embryos at E16.5. We did not observe a notable difference in staining for apoptotic

marker caspase 3, in either facial or palatine processes, indicating that a reduction in proliferation underlies the reduced size of both the nasal process as well as palatal shelves. Of note, we also found that the palatal shelves did not elevate in either *Esrp1*$^{-/-}$ or *Esrp1*$^{flox/flox}$*; Crect*$^{+/-}$ embryos (see also Fig. 1A). However, at this stage we cannot be certain that there is also a defect in palatal elevation independent of the palatal hypoplasia that contributes to cleft secondary palate.

We used a time series analysis of both WT and *Esrp1*$^{-/-}$ embryos during several stages of lip formation. Despite reduced proliferation, we noted several stages at which the MNP and LNP in *Esrp1*$^{-/-}$ embryos were able to make contact and adhere, but that this did not lead to apparent fusion by E12.5, at which point fusion was complete between the LNP, MNP, and MxP in WT embryos. While we were unable to successfully complete *ex vivo* facial explant cultures to further verify a fusion defect between MNP, LNP, and MxP, our studies using *ex vivo* palatal explants demonstrated that a fusion defect in *Esrp1*$^{-/-}$ embryos contributes to cleft palate. Since it is believed that the mechanisms of lip and palate fusion during development are similar (Jiang et al., 2006; Ray and Niswander, 2012), we believe that the fusion defect observed in palatal explants, taken together with our histology and SEM time course also indicate a defect in fusion during lip and primary palate formation.

We carried out in depth RNA-Seq analysis to identify alternative splicing changes in *Esrp1*$^{-/-}$ ectoderm and to define differences in splicing between wild-type ectoderm and mesenchyme. Numerous changes in splicing were identified in KO vs. WT ectoderm including some events that had previously been identified in *Esrp1*$^{-/-}$ epidermis, but the greater sequencing depth in this study identified a greater number of splicing changes than our previous studies. We first identified ESRP1 (and its paralog ESRP2) in a screen for regulators of *Fgfr2* splicing and, not surprisingly, one of the largest changes in splicing was a nearly complete switch in *Fgfr2* isoforms from Fgfr2-IIIb to Fgfr2-IIIc in *Esrp1* ablated ectoderm. This nearly complete change in splicing of Fgfr2 was in contrast to our analysis in E18.5 epidermis that examined changes in splicing in both *Esrp1*$^{-/-}$ and well as *Esrp1*$^{-/-}$*;Esrp2*$^{-/-}$ (double KO, or DKO) tissue, where there was no change in *Fgfr2* splicing unless both *Esrp1* and *Esrp2* were ablated (Bebee et al., 2015). This observation likely reflects the lower expression levels of both *Esrp1* and *Esrp2* in E12.0 surface ectoderm compared to E18.5 epidermis, including a significantly lower *Esrp2* expression level compared to *Esrp1* in ectoderm (see Table S3). We noted similar examples where deletion of *Esrp1* alone caused greater changes in splicing in ectoderm compared to the epidermis of *Esrp1*$^{-/-}$ mice and suspect that compensation by higher *Esrp2* levels in other tissues prevents most of the other major defects described in *Esrp1*$^{-/-}$*;Esrp2*$^{-/-}$ mice. We did note additional craniofacial abnormalities in *Esrp1*$^{-/-}$*;Esrp2*$^{-/-}$ mice, including mandibular defects, not seen in *Esrp1*$^{-/-}$ mice indicating that ESRP1-regulated splicing by both paralogs plays broader roles in craniofacial development (Bebee et al., 2015). A previous study demonstrated cleft palate, but not cleft lip, in mice in which the epithelial *Fgfr2* exon IIIb was deleted (Rice et al., 2004). However, deletion of exon IIIb in the mice did not default to splicing of exon IIIc in epithelial cells, but caused skipping of both exons and a frameshift that effectively resulted in no *Fgfr2* expression in epithelial

cells (De Moerlooze et al., 2000). In contrast, ablation of *Esrp1* induces a switch in isoforms, such that ectopic FGFR2-IIIc in epithelial cells can still respond to Fgf ligands to sustain Fgf signaling as we demonstrated in a prior study (Rohacek et al., 2017). These observations strongly suggest that altered splicing of *Fgfr2* does not account for the cleft lip observed in *Esrp1*$^{-/-}$ mice and is also unlikely, by itself, to cause cleft palate.

While we identified large numbers of splicing changes in *Esrp1*$^{-/-}$ compared to WT ectoderm, we also identified differences in splicing between WT ectoderm and WT mesenchyme. These analyses identified a large number of differences in splicing between these cell populations, which included many ESRP1 regulated events. We note that while numerous investigations have identified distinct epithelial and mesenchymal markers at the whole transcript or protein level, there remain limited examples in which large scale differences in splicing between these cell populations have been identified (Venables et al., 2013). The analysis presented here thus provides another resource to identify how different splice isoforms influence epithelial-mesenchymal crosstalk as previously described for *Fgfr2* (De Moerlooze et al., 2000; Warzecha et al., 2009a).

Identification of changes in total transcript levels in *Esrp1*$^{-/-}$ ectoderm compared to controls revealed substantial numbers of genes that were upregulated or downregulated and there was little if any overlap between these genes and those that demonstrated changes in splicing. Among these genes we noted decreases in the expression level of canonical Wnts, including *Wnt9b*, as well as *Shh*; components of two pathways that have previously been shown to be essential for lip and/or palate development (Jin et al., 2012; Lan and Jiang, 2009; Lipinski et al., 2010). These alterations are associated with corresponding downregulation of both canonical Wnt as well as Shh regulated targets in adjacent mesenchyme, suggesting that a reduction in a communication pathway from ectoderm to mesenchyme leads to reduced mesenchymal proliferation. Alterations in canonical Wnt signaling have been implicated in mouse models as well as human cases of syndromic and non-syndromic cleft lip and/or cleft palate (Reynolds et al., 2019), including CL/P in mice with ablation of *Wnt9b* and *Lrp6* (Carroll et al., 2005; Ferretti et al., 2011; Jin et al., 2012; Juriloff et al., 2006; Song et al., 2009). The reduced mesenchymal proliferation observed in mesenchyme of *Esrp1*$^{-/-}$ mice is similar to that demonstrated in both *Lrp6*$^{-/-}$ mice and *Wnt9b*$^{-/-}$ mice, suggesting that a decrease in Wnt signaling may, at least in part, contribute to reduced mesenchymal proliferation and failed approximation of the MNP, LNP, and MxP in *Esrp1*$^{-/-}$ mice. However, *Wnt9b*$^{-/-}$ mice did not have a defect in fusion of NP and MxP in explant cultures, whereas *Esrp1*$^{-/-}$ mice have a fusion defect in addition to reduced mesenchymal proliferation. Hence, we suspect that alterations in other genes and pathways prevent epithelial fusion in *Esrp1*$^{-/-}$ mice.

Previous studies have identified crosstalk between Wnt and hedgehog signaling and ablation of Shh in palatal epithelial cells or in utero treatment with Shh inhibitors, have been shown to cause cleft palate and CL/P, respectively (Lan and Jiang, 2009; Lipinski et al., 2010; Reynolds et al., 2019; Rice et al., 2004). It is thus possible that reduction in Shh expression in ectoderm might also

contribute to CL/P in *Esrp1* KO mice. We noted that in addition to reductions in Gli transcription factors, there was also reduced expression of *Foxf1a*, *Foxf2*, and *Osr2* in *Esrp1*$^{-/-}$ mesenchyme, which were previously shown to be downregulated in mesenchyme when Shh signaling from epithelial to mesenchyme cells caused cleft palate through ablation of *Smo* in mesenchyme (Lan and Jiang, 2009). These findings are also potentially relevant relevant to CL/P as another study showed that inhibition of Shh signaling with the inhibitor cyclopamine caused cleft lip that was also associated with a reduction of *Gli1* and *Foxf2* in mesenchyme of MNP (Everson et al., 2017). A recent study using single cell RNA-Seq to identify subpopulations of cell types present at the lambdoidal junction where the MNP, LNP, and MxP fuse characterized distinct and dynamic expression patterns in subsets of both ectodermal and mesenchymal cells during lip fusion (Li et al., 2019). This analysis revealed that while canonical Wnts were specifically expressed in the ectoderm of these processes, they were excluded from the fusion zone once these processes made contact, consistent with a lack of requirement for Wnts (at least for Wnt9b) for fusion and dissolution of the epithelial seam. This study also identified *Fgf10* among the genes that are highly expressed in mesenchymal cells at the fusion zone. During palate formation mesenchymal *Fgf10* was previously shown to induce *Shh* expression in adjacent epithelial cells via the Fgfr2-IIIb isoform and conditional ablation of *Shh* in palatal epithelial cells leads to cleft palate (Lan and Jiang, 2009). A switch in *Fgfr2* splicing in *Esrp1*$^{-/-}$ palatal epithelium would render it unresponsive to mesenchymal FGF10 suggesting that the *Fgfr2* splicing switch may be one factor leading to reduced *Shh* expression in epithelial cells of the facial processes as well as palate. In addition to *Fgf10*, the aforementioned single cell RNA-Seq analysis also showed a reduction of *Tgfb2* in the fusion zone of both ectoderm and mesenchyme (Li et al., 2019). It is therefore tempting to speculate that the reduction in *Tgfb2* observed in mesenchyme adjacent to *Esrp1*$^{-/-}$ ectoderm may contribute to the observed fusion defect. However, there may also be combinatorial effects of ectodermal genes that are upregulated upon *Esrp1* ablation, which includes *Dkk1*, *Aldha3*, and *Sfrs2* that have been described as Wnt inhibitors.

While our results suggest that reductions in Wnt signaling may be one factor contributing to CL/P in *Esrp1*$^{-/-}$ mice, an unresolved question remains as to how *Esrp1* ablation in ectoderm leads to coordinated changes in the expression of several canonical Wnts. Ablation of the *Pbx1* and *Pbx2* transcription factors was previously shown to lead to CL/P through reduced expression of *Wnt9b* and *Wnt3*. However, we did not identify changes in the expression of *Pbx1*, *Pbx2*, or *Pbx3* in *Esrp1*$^{-/-}$ ectoderm. While there is a vast literature describing numerous Wnt target genes in different contexts, there is limited understanding as to how the Wnt genes themselves are transcriptionally regulated. We suspect that changes in transcriptional regulation that result from *Esrp1* ablation are indirect; possibly through alterations in signaling pathways that regulate transcription factor expression and/or activity.

A major challenge for future studies will be to decipher the molecular mechanisms by which loss of *Esrp1* leads to alterations in components of numerous pathways that have been linked to clefting disorders (Table S6). These include, but are not limited to, WNT. SHH, TGFβ, BMP, FGF,

and Hippo pathways. Future studies are needed to define the relative contributions of alterations in each of these signaling pathways in CL/P in these mice. The transcriptomic analysis presented here will hopefully provide a resource that can be used by the community to further explore the molecular mechanisms that lead to CL/P as well as *Esrp1* regulated targets that merit further investigations as possible disease genes.

MATERIALS and METHODS

Mouse strains

Generation of *Esrp1* KO *(Esrp1*$^{-/-}$*)* and Conditional *Esrp1* (*Esrp1*$^{flox/flox}$) were described previously (Bebee et al., 2015) as was the *Crect* strain (Reid et al., 2011). *Axin2*^{LacZ} (Manuylov et al., 2008) and *TCF/Lef1:H2B-GFP* (Ferrer-Vaquer et al., 2010) strains were purchased from JAX Labs (Bar Harbor, ME). *Esrp1*$^{FLAG/FLAG}$ mice were generated in mouse V6.5 ES cells by the Penn Transgenic and Chimeric mouse core facility using electroporation of an mRNA encoding Cas9, a sgRNA targeting the ATG start codon, and an oligonucleotide repair template encoding two tandem copies of the FLAG epitope tag. *Esrp1*^{Triaka} mice were described previously (Mager et al., 2017). Relevant strains were interbred from embryo isolation and females were examined in the morning for presence of a vaginal plug, and the presence of a plug was designated E0.5. Genomic DNA for genotyping was derived from tail biopsies and genotyping was performed using standard procedures for these strains. Both male and female mice and embryos were used in this study. All animal procedures and experiments were approved by the Institutional Animal Care and Use Committee (IACUC) at the University of Pennsylvania.

Scanning Electron Microscopy.

Mouse embryos were harvested at either E10.5, E11.5, or E12.5. The heads were fixed in Karnovsky's solution and a portion of the unfixed body including the tail was saved from each embryo for genotyping. Fixed head samples were dehydrated through a graded ethanol series and placed in Freon (1,1,2-Trichloro-1,2,2 Trifluoroethane) (Recycle & Reuse Industries, Mansfield, TX) for critical-point drying. The samples were mounted on aluminum stubs with clay and sputter-coated with gold in an Argon atmosphere, using a Denton Vacuum Desk II Cold Sputter Etch Unit (Denton Vacuum, Cherry Hill, NJ). The heads were then viewed under a Quanta 600 FEG Mark II scanning electron microscope (FEI, Hillsboro, OR).

Isolation of ectoderm and mesenchyme for RNA harvest

E12.0 mouse embryos were dissected, and the ectodermal and mesenchymal tissue layers of the prominences were separated and collected for wild-type and *Esrp1*$^{-/-}$ mice for a total of 4 pools of 6 to 7 mice in each category. The facial ectoderm and mesenchyme of each embryo was separated using a described surgical protocol (Li and Williams, 2013). RNA harvest of collected tissue was described previously (Bebee et al., 2015). For synthesis of cDNA, 300ng of total RNA was used for ectoderm and mesenchyme samples, oligodT primer, and SuperScript3 reverse transcriptase (Invitrogen, Carlsbad, CA).

Real time RT-PCR and RT-PCR

Real-time RT-PCR and RT-PCR were performed as described (Bebee et al., 2015; Lee et al., 2018). Briefly, Real-time RT-PCR analysis were quantified using ImageQuant TL, version 7.0. Splicing ratios are represented as PSI for cassette exons and were normalized to RT-PCR product size. Real-time RT-PCR and RT-PCR primer sequences are listed in Supplemental Table S6 and Supplemental Table S7.

RNA-Sequencing and data analysis

Total RNA from ectodermal and mesenchymal samples was used for RNA-Seq at the Penn Next Generation Sequencing Core (NGSC) Facility as previously described with the exception that we obtained 150 bp paired end reads (Bebee et al., 2015). The average number of read pairs was approximately 100 million read pairs per replicate. Identification of changes in alternative splicing in ectoderm samples was carried out using rMATS as previously described (Shen et al., 2014). Differential gene expression analysis was carried out by the Penn NGSC using EdgeR. Gene expression values were measured by Kallisto (v0.43.0) with mm10 gencode vM13 as the transcriptome index. Gene Ontology and pathway analysis was conducted using DAVID (Huang et al., 2007).

Data Availability

The RNA-seq data has been deposited into the NCBI Gene Expression Omnibus under accession GSE144853.

Skeletal analysis

E18.5 embryo heads were skinned, fixed in 4% Paraformaldehyde O/N. For cartilage and bone staining, E18.5 embryos were stained with Alizarin red and Alcian blue for examination of bone and cartilage structure, as previously described (Bebee et al., 2015).

Histology and Immunofluorescence

Embryos from E10.5 to E14.5 were harvested and fixed O/N at 4% in PFA and fixed in paraffin. Paraffin sections were deparaffinized in xylene and rehydrated using a graded ethanol series. For standard histology sections were stained with H & E. For immunofluorescence, antigen retrieval was performed using unmasking solution (Vector Laboratories, Burlingame, CA) in a humidified chamber. Samples were blocked with 5% BSA and 3% sheep serum in PBST 1hour at RT. Primary antibodies were incubated overnight at 4°C. After washing with PBST, secondary antibodies were applied for 30 minutes at RT, followed by another wash and mounted with Prolong Gold antifade reagent with DAPI (Invitrogen). Images were taken using an Olympus BX43. Samples were incubated with primary antibodies against FLAG-M2 (Sigma, Cat #F1804, 1:1000), E-cadherin (BD Bioscience, Cat #610181, 1:500), Cleaved Caspase-3 (Cell Signaling, #9664S, 1:500), Ki-67 (Abcam, Ab16667, 1:500), GFP (Abcam # A-11122, 1:1000), Beta Galactosidase (Abcam, ab9361, 1:1000) and secondary antibodies Rabbit IgG Alexa 488(Life technologies, Cat #A24922, 1:500), and Mouse IgG Alexa 594 (Life technologies, Cat #A24921, 1:500). Quantifications of fluorescence in immunostained slides was carried out using ImageJ with comparisons between tissues corrected for area

Whole-mount and Section In Situ hybridization

In situ hybridization experiments were carried out as previously described (Moorman et al., 2001; Warzecha et al., 2009a) using digoxigenin-labeled riboprobes for Axin2, Lef1, Wnt9b, Shh. The signal was detected with alkaline phosphatase and then color developed with BP substrate.

Palatal organ culture

A pair of unfused palatal shelves were dissected out from an E14 mouse embryo under a dissecting microscope and placed on autoclaved nitrocellulose membrane with the oral side facing down. The palatal shelves were correctly oriented as in vivo and gently pushed against each other to ensure contact between the medial edge epithelia. Palatal shelves on a membrane were rested on a wire grid in 12 well culture plate and cultured for 72 hours in DMEM containing 10% FBS. Tail DNA isolated from each embryo was used for genotyping. The organ culture was then processed for histology and immunofluorescent labeling.

Acknowledgements

We thank Natoya Peart, Eric C. Liao, and Shannon Carroll for critical review of the manuscript. We are grateful to the Transgenic and Chimeric Mouse Core of the University of Pennsylvania for generation of *Esrp1*$^{FLAG/FLAG}$ mice (supported by NIH center grants P30DK050306, P30DK019525, and P30CA016520) We thank Lukas F. Mager and Lester Thoo (University of Bern) for organizing neonatal Triaka mice.

Competing interests

Yi Xing is a scientific cofounder of Panorama Medicine. All other authors declare no competing interests.

Author contributions

S.L.K. performed most experiments. M.J.S, I.S., and H.D.N performed some of the experiments. H.L. and T.W provided direct training and reagents for the isolation of ectoderm and mesenchyme from E12.0 facial prominences. Z.Z. and Y.X. carried out the processing of the RNA-Seq data using rMATS for alternative splicing analysis. P. K. supervised studies of *Esrp1*$^{Triaka/-}$ mice that analyzed facial and palatal development. R.P. C. and S.K.L. conceived, designed the study, and wrote the manuscript.

Funding

This work was supported by NIH grants R56-DE024749, R01-DE024749, P30-AR050950 (R.P.C.) and 1U01DE024429 (T.W.).

References

Bebee, T. W., Park, J. W., Sheridan, K. I., Warzecha, C. C., Cieply, B. W., Rohacek, A. M., Xing, Y. and Carstens, R. P. (2015). The splicing regulators Esrp1 and Esrp2 direct an epithelial splicing program essential for mammalian development. *Elife* **4**.

Braeutigam, C., Rago, L., Rolke, A., Waldmeier, L., Christofori, G. and Winter, J. (2014). The RNA-binding protein Rbfox2: an essential regulator of EMT-driven alternative splicing and a mediator of cellular invasion. *Oncogene* **33**, 1082-1092.

Carroll, T. J., Park, J. S., Hayashi, S., Majumdar, A. and McMahon, A. P. (2005). Wnt9b plays a central role in the regulation of mesenchymal to epithelial transitions underlying organogenesis of the mammalian urogenital system. *Developmental cell* **9**, 283-292.

De Moerlooze, L., Spencer-Dene, B., Revest, J., Hajihosseini, M., Rosewell, I. and Dickson, C. (2000). An important role for the IIIb isoform of fibroblast growth factor receptor 2 (FGFR2) in mesenchymal-epithelial signalling during mouse organogenesis. *Development* **127**, 483-492.

Dixon, M. J., Marazita, M. L., Beaty, T. H. and Murray, J. C. (2011). Cleft lip and palate: understanding genetic and environmental influences. *Nature reviews. Genetics* **12**, 167-178.

Everson, J. L., Fink, D. M., Yoon, J. W., Leslie, E. J., Kietzman, H. W., Ansen-Wilson, L. J., Chung, H. M., Walterhouse, D. O., Marazita, M. L. and Lipinski, R. J. (2017). Sonic hedgehog regulation of Foxf2 promotes cranial neural crest mesenchyme proliferation and is disrupted in cleft lip morphogenesis. *Development* **144**, 2082-2091.

Ferrer-Vaquer, A., Piliszek, A., Tian, G., Aho, R. J., Dufort, D. and Hadjantonakis, A. K. (2010). A sensitive and bright single-cell resolution live imaging reporter of Wnt/ss-catenin signaling in the mouse. *BMC Dev Biol* **10**, 121.

Ferretti, E., Li, B., Zewdu, R., Wells, V., Hebert, J. M., Karner, C., Anderson, M. J., Williams, T., Dixon, J., Dixon, M. J., et al. (2011). A conserved Pbx-Wnt-p63-Irf6 regulatory module controls face morphogenesis by promoting epithelial apoptosis. *Developmental cell* **21**, 627-641.

Fraser, F. C. (1970). The genetics of cleft lip and cleft palate. *American journal of human genetics* **22**, 336-352.

Green, R. M., Feng, W., Phang, T., Fish, J. L., Li, H., Spritz, R. A., Marcucio, R. S., Hooper, J., Jamniczky, H., Hallgrimsson, B., et al. (2015). Tfap2a-dependent changes in mouse facial morphology result in clefting that can be ameliorated by a reduction in Fgf8 gene dosage. *Disease models & mechanisms* **8**, 31-43.

Gritli-Linde, A. (2008). The etiopathogenesis of cleft lip and cleft palate: usefulness and caveats of mouse models. *Current topics in developmental biology* **84**, 37-138.

---- (2012). The mouse as a developmental model for cleft lip and palate research. *Frontiers of oral biology* **16**, 32-51.

Huang, D. W., Sherman, B. T., Tan, Q., Kir, J., Liu, D., Bryant, D., Guo, Y., Stephens, R., Baseler, M. W., Lane, H. C., et al. (2007). DAVID Bioinformatics Resources: expanded annotation database and novel algorithms to better extract biology from large gene lists. *Nucleic Acids Res* **35**, W169-175.

Jiang, R., Bush, J. O. and Lidral, A. C. (2006). Development of the upper lip: morphogenetic and molecular mechanisms. *Developmental dynamics : an official publication of the American Association of Anatomists* **235**, 1152-1166.

Jin, Y. R., Han, X. H., Taketo, M. M. and Yoon, J. K. (2012). Wnt9b-dependent FGF signaling is crucial for outgrowth of the nasal and maxillary processes during upper jaw and lip development. *Development* **139**, 1821-1830.

Juriloff, D. M. and Harris, M. J. (2008). Mouse genetic models of cleft lip with or without cleft palate. *Birth defects research. Part A, Clinical and molecular teratology* **82**, 63-77.

Juriloff, D. M., Harris, M. J., McMahon, A. P., Carroll, T. J. and Lidral, A. C. (2006). Wnt9b is the mutated gene involved in multifactorial nonsyndromic cleft lip with or without cleft palate in A/WySn mice, as confirmed by a genetic complementation test. *Birth defects research. Part A, Clinical and molecular teratology* **76**, 574-579.

Kaartinen, V., Voncken, J. W., Shuler, C., Warburton, D., Bu, D., Heisterkamp, N. and Groffen, J. (1995). Abnormal lung development and cleft palate in mice lacking TGF-beta 3 indicates defects of epithelial-mesenchymal interaction. *Nat Genet* **11**, 415-421.

Kalsotra, A. and Cooper, T. A. (2011). Functional consequences of developmentally regulated alternative splicing. *Nature reviews. Genetics* **12**, 715-729.

Kouskoura, T., Kozlova, A., Alexiou, M., Blumer, S., Zouvelou, V., Katsaros, C., Chiquet, M., Mitsiadis, T. A. and Graf, D. (2013). The etiology of cleft palate formation in BMP7-deficient mice. *PloS one* **8**, e59463.

Lan, Y. and Jiang, R. (2009). Sonic hedgehog signaling regulates reciprocal epithelial-mesenchymal interactions controlling palatal outgrowth. *Development* **136**, 1387-1396.

Lee, S., Cieply, B., Yang, Y., Peart, N., Glaser, C., Chan, P. and Carstens, R. P. (2018). Esrp1-Regulated Splicing of Arhgef11 Isoforms Is Required for Epithelial Tight Junction Integrity. *Cell Rep* **25**, 2417-2430 e2415.

Li, C., Lan, Y. and Jiang, R. (2017). Molecular and Cellular Mechanisms of Palate Development. *J Dent Res* **96**, 1184-1191.

Li, H., Jones, K. L., Hooper, J. E. and Williams, T. (2019). The molecular anatomy of mammalian upper lip and primary palate fusion at single cell resolution. *Development* **146**.

Li, H. and Williams, T. (2013). Separation of mouse embryonic facial ectoderm and mesenchyme. *Journal of visualized experiments : JoVE*.

Lipinski, R. J., Song, C., Sulik, K. K., Everson, J. L., Gipp, J. J., Yan, D., Bushman, W. and Rowland, I. J. (2010). Cleft lip and palate results from Hedgehog signaling antagonism in the mouse: Phenotypic characterization and clinical implications. *Birth defects research. Part A, Clinical and molecular teratology* **88**, 232-240.

Liu, W., Sun, X., Braut, A., Mishina, Y., Behringer, R. R., Mina, M. and Martin, J. F. (2005). Distinct functions for Bmp signaling in lip and palate fusion in mice. *Development* **132**, 1453-1461.

Mager, L. F., Koelzer, V. H., Stuber, R., Thoo, L., Keller, I., Koeck, I., Langenegger, M., Simillion, C., Pfister, S. P., Faderl, M., et al. (2017). The ESRP1-GPR137 axis contributes to intestinal pathogenesis. *Elife* **6**.

Manuylov, N. L., Smagulova, F. O., Leach, L. and Tevosian, S. G. (2008). Ovarian development in mice requires the GATA4-FOG2 transcription complex. *Development* **135**, 3731-3743.

Moorman, A. F., Houweling, A. C., de Boer, P. A. and Christoffels, V. M. (2001). Sensitive nonradioactive detection of mRNA in tissue sections: novel application of the whole-mount in situ hybridization protocol. *J Histochem Cytochem* **49**, 1-8.

Osei-Sarfo, K. and Gudas, L. J. (2014). Retinoic acid suppresses the canonical Wnt signaling pathway in embryonic stem cells and activates the noncanonical Wnt signaling pathway. *Stem Cells* **32**, 2061-2071.

Pillman, K. A., Phillips, C. A., Roslan, S., Toubia, J., Dredge, B. K., Bert, A. G., Lumb, R., Neumann, D. P., Li, X., Conn, S. J., et al. (2018). miR-200/375 control epithelial plasticity-associated alternative splicing by repressing the RNA-binding protein Quaking. *EMBO J* **37**.

Proetzel, G., Pawlowski, S. A., Wiles, M. V., Yin, M., Boivin, G. P., Howles, P. N., Ding, J., Ferguson, M. W. and Doetschman, T. (1995). Transforming growth factor-beta 3 is required for secondary palate fusion. *Nat Genet* **11**, 409-414.

Ray, H. J. and Niswander, L. (2012). Mechanisms of tissue fusion during development. *Development* **139**, 1701-1711.

Reid, B. S., Yang, H., Melvin, V. S., Taketo, M. M. and Williams, T. (2011). Ectodermal Wnt/beta-catenin signaling shapes the mouse face. *Dev Biol* **349**, 261-269.

Revil, T. and Jerome-Majewska, L. A. (2013). During embryogenesis, esrp1 expression is restricted to a subset of epithelial cells and is associated with splicing of a number of developmentally important genes. *Developmental dynamics : an official publication of the American Association of Anatomists* **242**, 281-290.

Reynolds, K., Kumari, P., Sepulveda Rincon, L., Gu, R., Ji, Y., Kumar, S. and Zhou, C. J. (2019). Wnt signaling in orofacial clefts: crosstalk, pathogenesis and models. *Disease models & mechanisms* **12**.

Rice, R., Spencer-Dene, B., Connor, E. C., Gritli-Linde, A., McMahon, A. P., Dickson, C., Thesleff, I. and Rice, D. P. (2004). Disruption of Fgf10/Fgfr2b-coordinated epithelial-mesenchymal interactions causes cleft palate. *J Clin Invest* **113**, 1692-1700.

Rohacek, A. M., Bebee, T. W., Tilton, R. K., Radens, C. M., McDermott-Roe, C., Peart, N., Kaur, M., Zaykaner, M., Cieply, B., Musunuru, K., et al. (2017). ESRP1 Mutations Cause Hearing Loss due to Defects in Alternative Splicing that Disrupt Cochlear Development. *Dev Cell* **43**, 318-331 e315.

Sanford, L. P., Ormsby, I., Gittenberger-de Groot, A. C., Sariola, H., Friedman, R., Boivin, G. P., Cardell, E. L. and Doetschman, T. (1997). TGFbeta2 knockout mice have multiple developmental defects that are non-overlapping with other TGFbeta knockout phenotypes. *Development* **124**, 2659-2670.

Shapiro, I. M., Cheng, A. W., Flytzanis, N. C., Balsamo, M., Condeelis, J. S., Oktay, M. H., Burge, C. B. and Gertler, F. B. (2011). An EMT-driven alternative splicing program occurs in human breast cancer and modulates cellular phenotype. *PLoS Genet* **7**, e1002218.

Shen, S., Park, J. W., Lu, Z. X., Lin, L., Henry, M. D., Wu, Y. N., Zhou, Q. and Xing, Y. (2014). rMATS: robust and flexible detection of differential alternative splicing from replicate RNA-Seq data. *Proceedings of the National Academy of Sciences of the United States of America* **111**, E5593-5601.

Song, L., Li, Y., Wang, K., Wang, Y. Z., Molotkov, A., Gao, L., Zhao, T., Yamagami, T., Wang, Y., Gan, Q., et al. (2009). Lrp6-mediated canonical Wnt signaling is required for lip formation and fusion. *Development* **136**, 3161-3171.

Ule, J., Ule, A., Spencer, J., Williams, A., Hu, J. S., Cline, M., Wang, H., Clark, T., Fraser, C., Ruggiu, M., et al. (2005). Nova regulates brain-specific splicing to shape the synapse. *Nat Genet* **37**, 844-852.

Venables, J. P., Brosseau, J. P., Gadea, G., Klinck, R., Prinos, P., Beaulieu, J. F., Lapointe, E., Durand, M., Thibault, P., Tremblay, K., et al. (2013). RBFOX2 is an important regulator of mesenchymal tissue-specific splicing in both normal and cancer tissues. *Mol Cell Biol* **33**, 396-405.

Warzecha, C. C., Sato, T. K., Nabet, B., Hogenesch, J. B. and Carstens, R. P. (2009a). ESRP1 and ESRP2 are epithelial cell-type-specific regulators of FGFR2 splicing. *Mol Cell* **33**, 591-601.

Warzecha, C. C., Shen, S., Xing, Y. and Carstens, R. P. (2009b). The epithelial splicing factors ESRP1 and ESRP2 positively and negatively regulate diverse types of alternative splicing events. *RNA biology* **6**, 546-562.

Wedden, S. E. (1987). Epithelial-mesenchymal interactions in the development of chick facial primordia and the target of retinoid action. *Development* **99**, 341-351.

Williamson, K. A., Rainger, J., Floyd, J. A., Ansari, M., Meynert, A., Aldridge, K. V., Rainger, J. K., Anderson, C. A., Moore, A. T., Hurles, M. E., et al. (2014). Heterozygous loss-of-function mutations in YAP1 cause both isolated and syndromic optic fissure closure defects. *American journal of human genetics* **94**, 295-302.

Yang, Y., Park, J. W., Bebee, T. W., Warzecha, C. C., Guo, Y., Shang, X., Xing, Y. and Carstens, R. P. (2016). Determination of a Comprehensive Alternative Splicing Regulatory Network and Combinatorial Regulation by Key Factors during the Epithelial-to-Mesenchymal Transition. *Mol Cell Biol* **36**, 1704-1719.

Zhang, C., Zhang, Z., Castle, J., Sun, S., Johnson, J., Krainer, A. R. and Zhang, M. Q. (2008). Defining the regulatory network of the tissue-specific splicing factors Fox-1 and Fox-2. *Genes Dev* **22**, 2550-2563.

Zhang, X., Ibrahimi, O. A., Olsen, S. K., Umemori, H., Mohammadi, M. and Ornitz, D. M. (2006). Receptor specificity of the fibroblast growth factor family. The complete mammalian FGF family. *J Biol Chem* **281**, 15694-15700.

Figures

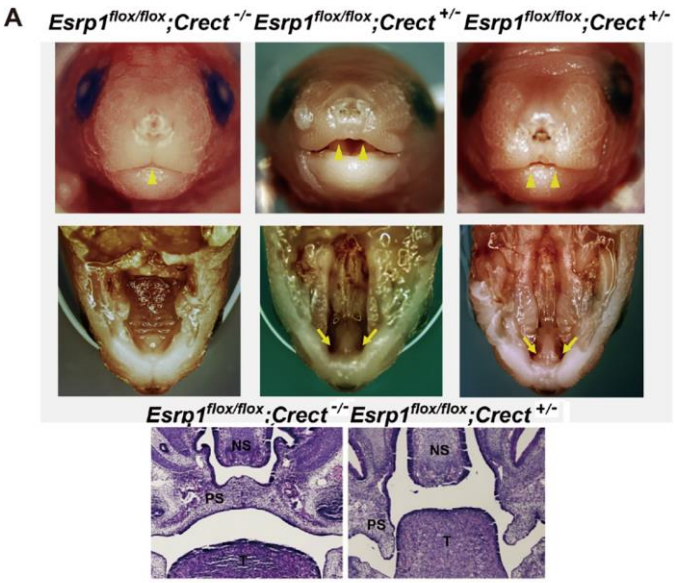

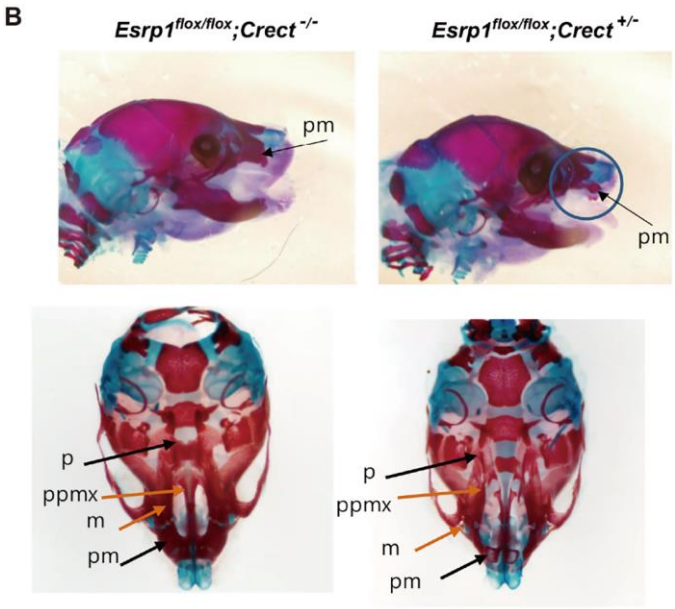

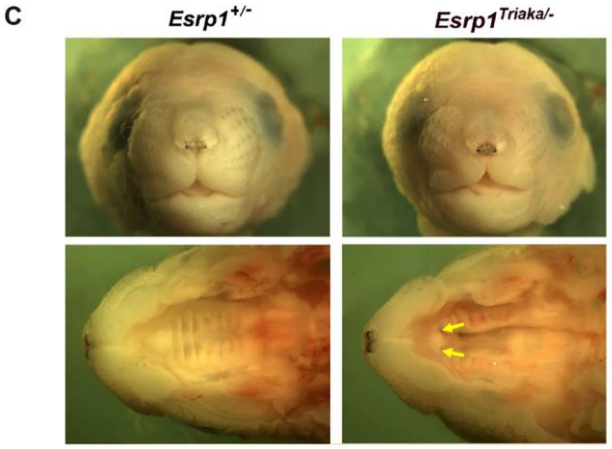

Fig. 1. Conditional ablation of *Esrp1* in surface ectoderm leads to CL/P. (A) Frontal views of control (*Esrp1*$^{flox/flox}$) and *Esrp1*$^{flox/flox}$*; Crect*$^{+/-}$ cKO E18.5 embryos showing that the midline philtrum observed in control mice (single arrowhead) is absent in cKO mice as the upper lip primordia fail to meet at the midline (double arrowheads). Views of the palate after removal of the mandible show clefting of the secondary palate and primary palate in cKO mutants (arrows). H & E images of coronal sections show hypoplastic palatal processes in *Esrp1*$^{flox/flox}$*; Crect*$^{+/-}$ embryos. PS, palatal shelf; NS, Nasal Septum; T, Tongue. (B) Alizarin Red/Alcian Blue stains of E18.5 embryos from the side (top) and the ventral side with mandible removed (bottom). Defects are apparent in the cKO maxilla (m), palatine (p), premaxilla (pm), and palatal process of the maxilla (ppmx). (C) Frontal and ventral view with lower jaw removed of Esrp1$^{Triaka/-}$ mice without cleft lip or primary palate formation (arrows), but cleft secondary palate.

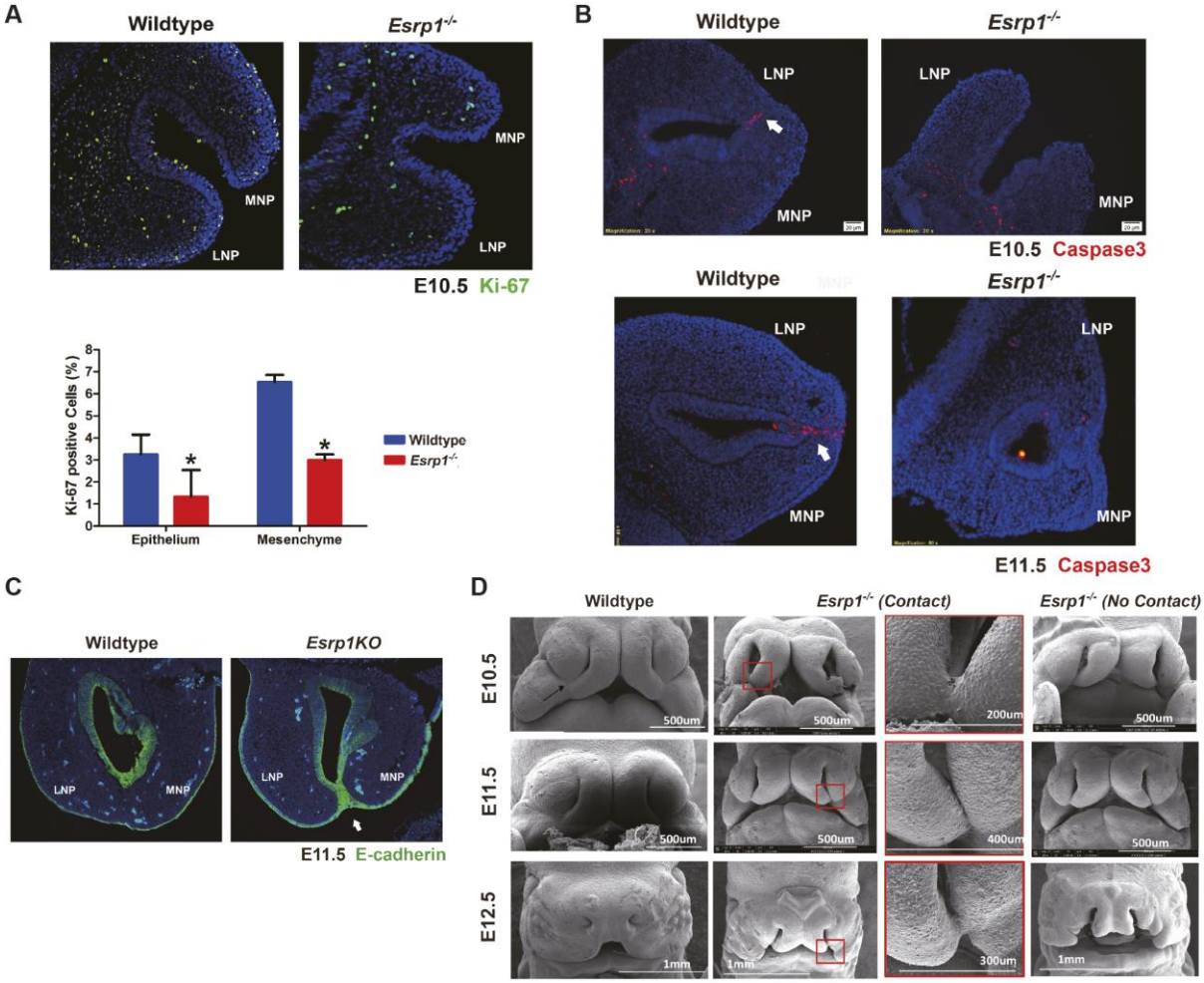

Fig. 2. *Esrp1*$^{-/-}$ embryos exhibit reduced proliferation of the MNP and LNP and do not fuse. (A) Frontal section showing decreased Ki-67 staining (green) in *Esrp1*$^{-/-}$ ectoderm and mesenchyme of *Esrp1*$^{-/-}$ embryos at E10.5 compared to controls. Quantifications of Ki-67 are shown from WT (N=3) and *Esrp1*$^{-/-}$ embryos (N=3). Y-axis indicates the % of Ki67 positive cells compared to total cells within each section. Error bars indicate s.d. Statistical significance was determined by two-tailed t-test. *P <0.05. (B) Arrow shows epithelial seam at fusion site between MNP and LNP in WT embryos showing the expected apoptosis by activated Caspase 3 staining (red). MNP and LNP from two Esrp1$^{-/-}$ embryos did not reveal substantial apoptosis, including one example where MNP and LNP make contact. Nuclei are stained with DAPI (blue) (C) E-Cadherin staining (green) showing loss of epithelial cells between MNP and LNP after fusion in WT embryos, but persistence in MNP and LNP making contact in *Esrp1*$^{-/-}$ embryos. (D) Scanning electron microscopy (SEM) showing normal lip fusion in WT embryos from E10.5 to E12.5. The arrow in the WT image at E10.5 shows the normal formation of the lambdoidal junction. In *Esrp1*$^{-/-}$ embryos we observed examples with no apparent contact between MNP and LNP or cases with contact, but none with fusion by E12.5. LNP, lateral nasal process; MNP, medial nasal process.

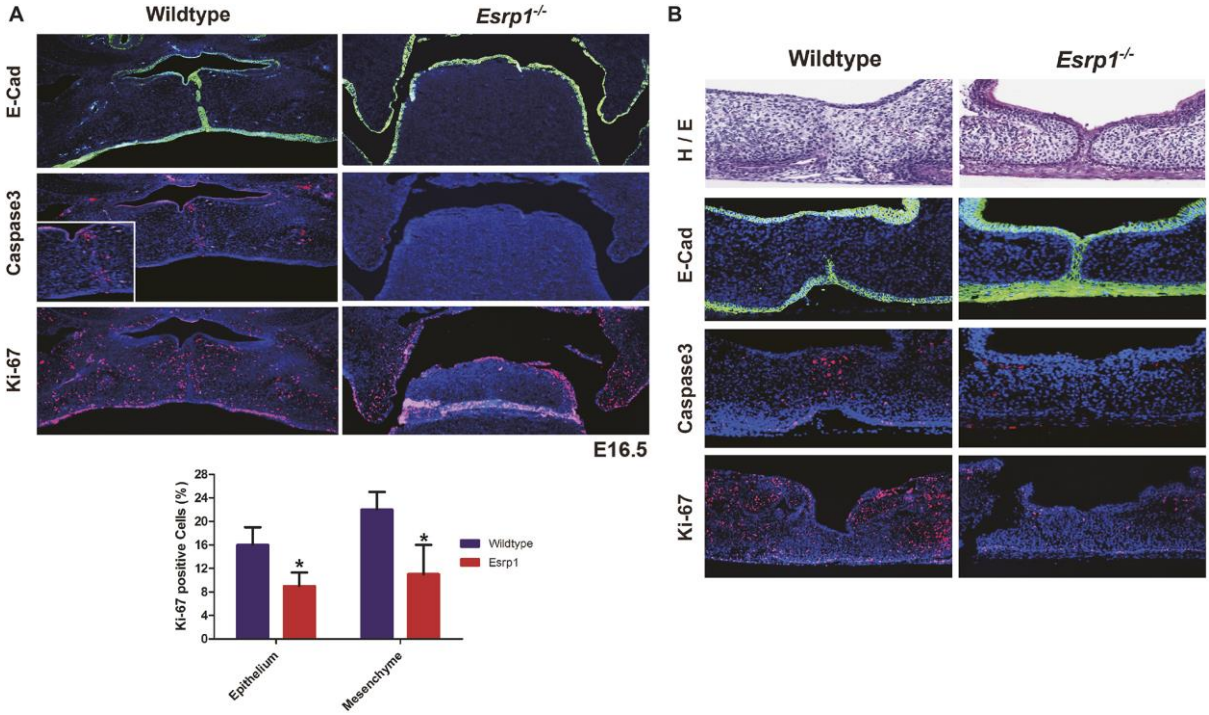

Fig. 3. Reduced proliferation and a fusion defect contribute to cleft palate in *Esrp1*$^{-/-}$ mice. (A) Coronal sections stained for E-cadherin (green) in E16.5 control and *Esrp1*$^{-/-}$ embryos showing the medial edge epithelial seam (MES) becoming discontinuous following fusion in controls whereas palatal shelves failed to elevate in the mutants. Activated Caspase 3 staining shows apoptosis at the site of fusion, but no apparent increase in apoptosis in *Esrp1*$^{-/-}$ embryos, which also show reduced Ki-67 staining for proliferating cells compared to WT in the palatal shelves. Quantifications are from WT (N=3) and *Esrp1*$^{-/-}$ embryos (N=3). Error bars indicate standard deviation. Statistical significance was determined by two tailed t-test. *P <0.05. Error bars indicate s.d. (B) Palatal organ culture showing lack of dissolution of the MES and associated apoptosis and reduced proliferation in palatal shelves from *Esrp1*$^{-/-}$ embryos compared to WT.

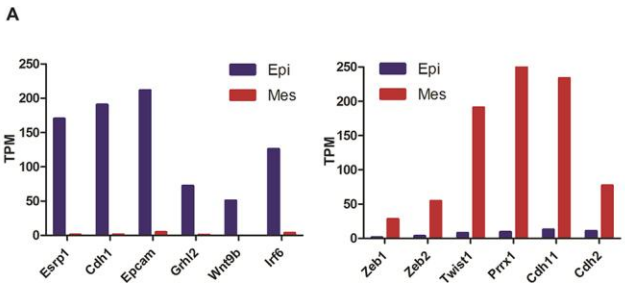

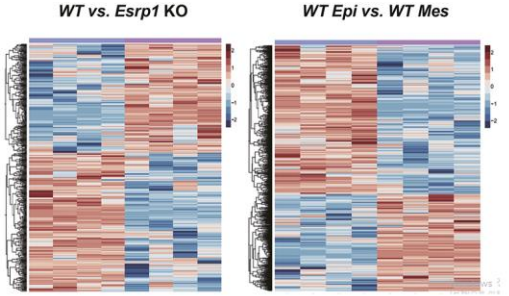

B

AS events	WT vs. Esrp1 KO
Skipped Exons (SE)	646 (44%)
Mutually Exclusive Exons (MXE)	461 (31%)
Alt. 5' splice sites (A5SS)	52 (4%)
Alt. 3' splice sites (A3SS)	88 (6%)
Retained Intron (RI)	220 (15%)
Total	1467

AS events	WT Epi vs. WT Mes
Skipped Exons (SE)	1609 (63%)
Mutually Exclusive Exons (MXE)	486 (19%)
Alt. 5' splice sites (A5SS)	113 (4%)
Alt. 3' splice sites (A3SS)	123 (5%)
Retained Intron (RI)	215 (8%)
Total	2546

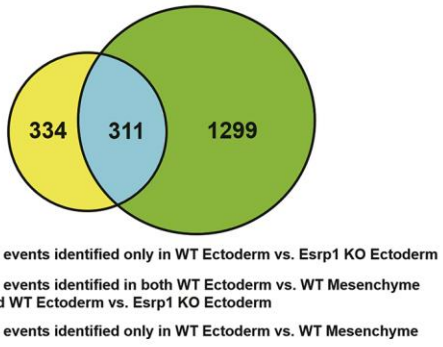

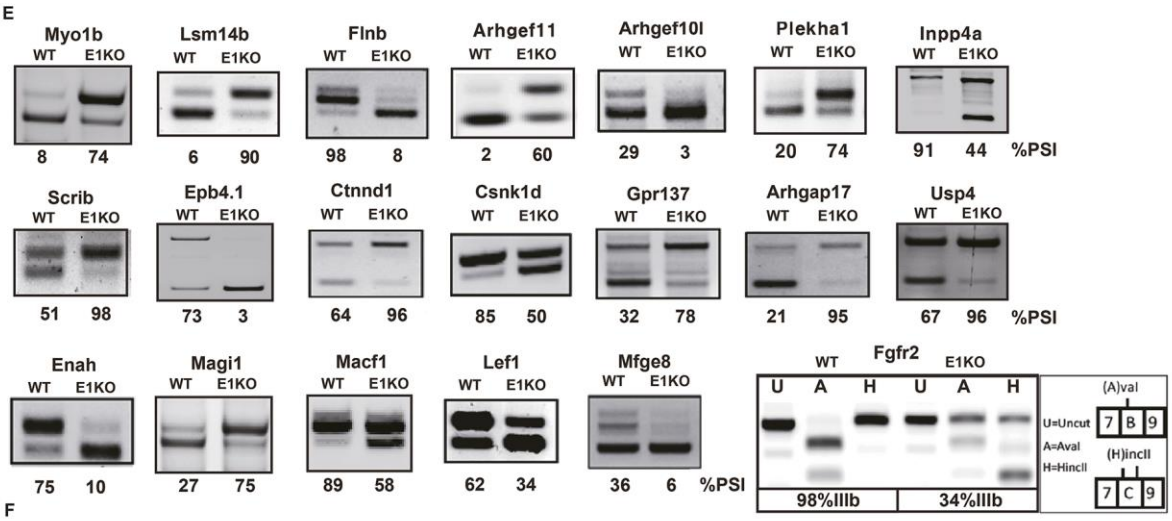

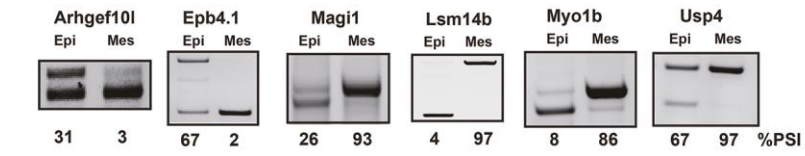

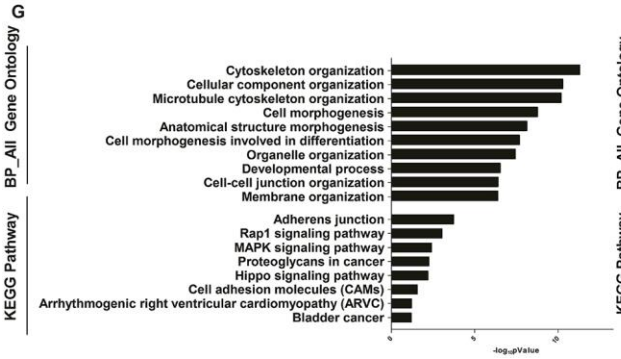

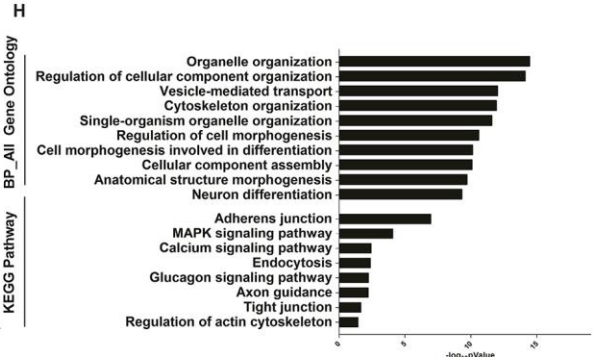

Fig. 4. RNA-Seq identified large scale alterations in alternative splicing in *Esrp1*$^{-/-}$ ectoderm compared to WT ectoderm and differences in alternative splicing between WT ectoderm and WT mesenchyme. (A) Expression epithelial markers (left) and mesenchymal markers (right) validates efficient separation of epithelial cells from mesenchymal cells in WT samples. TPM = transcripts per million. (B) Summary derived from Tables S1 and S2 showing both the total number and percentage of the different types of AS events in WT vs. *Esrp1*$^{-/-}$ ectoderm (top) and in WT ectoderm vs. WT mesenchyme (bottom) identified by MATS with False Discovery Rate (FDR) <5%, and |deltaPSI|>=5%. (C) Heatmap representing the skipped exon (SE) splicing changes with increased exon inclusion (red) or decreased exon inclusion (blue). (D) Venn diagram depicting detected SE events identified in WT ectoderm vs. *Esrp1* KO ectoderm (yellow), WT ectoderm vs. WT mesenchyme (green), and those identified in both comparison sets (blue). (E) RT-PCR validations of changes in splicing of cassette exons *Esrp1*$^{-/-}$ ectoderm (E1KO) compared to WT. The Percent Spliced In (PSI) value indicates % exon inclusion for each event. Also shown is the change in splicing of mutually exclusive exons IIIb and IIIc of Fgfr2. Products containing each exon were distinguished by restriction digests with Ava I and Hinc II, which cut products containing exon IIIb and IIIc, respectively. (F) Validation of several differences in splicing between control ectoderm and mesenchyme. (G) Gene Ontology (GO) and KEGG pathway enrichment for genes with alternative splicing differences between WT ectoderm and *Esrp1*$^{-/-}$ ectoderm. H. Gene Ontology (GO) and KEGG pathway enrichment for genes with splicing differences between WT ectoderm and WT mesenchyme.

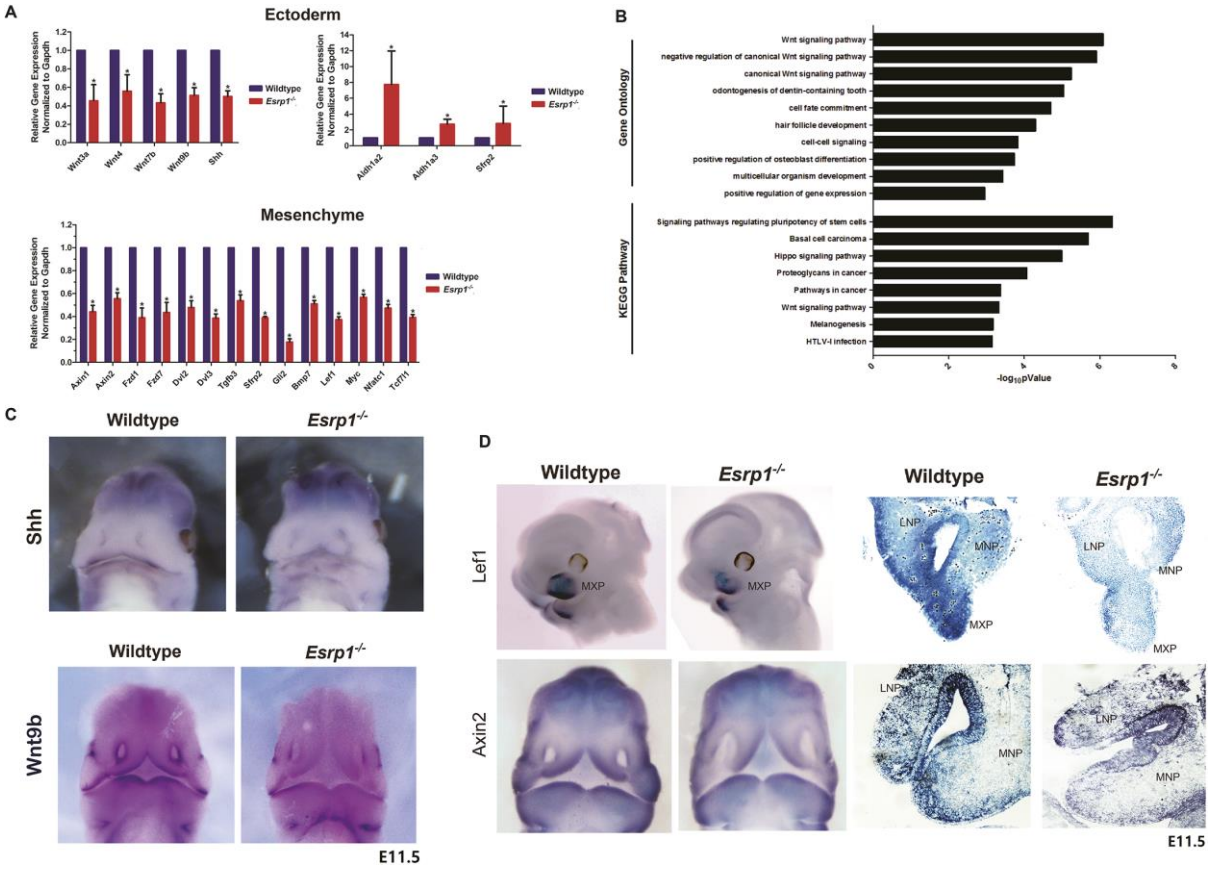

Fig. 5. *Esrp1* ablation in ectoderm results in altered expression of components of the Wnt signaling pathway and other signaling pathways implicated in cleft lip and/or cleft palate. (a) qRT-PCR validations for select changes in total transcript levels in *Esrp1*$^{-/-}$ ectoderm as well as in adjacent mesenchyme. Error bars indicate standard deviation. Statistical significance for each comparison was determined by two-tailed t-test. *P <0.05. (B) Gene Ontology (GO) and KEGG pathway enrichment for genes that are downregulated in *Esrp1*$^{-/-}$ ectoderm. (C) Whole mount in situ hybridization of E11.5 embryos showing reduced expression of *Shh* and *Wnt9b* in epithelial cells of the developing face. (D) Whole mount and tissue sections showing reduced expression of canonical Wnt target genes *Lef1* and *Axin2* in *Esrp1*$^{-/-}$ embryos.

A

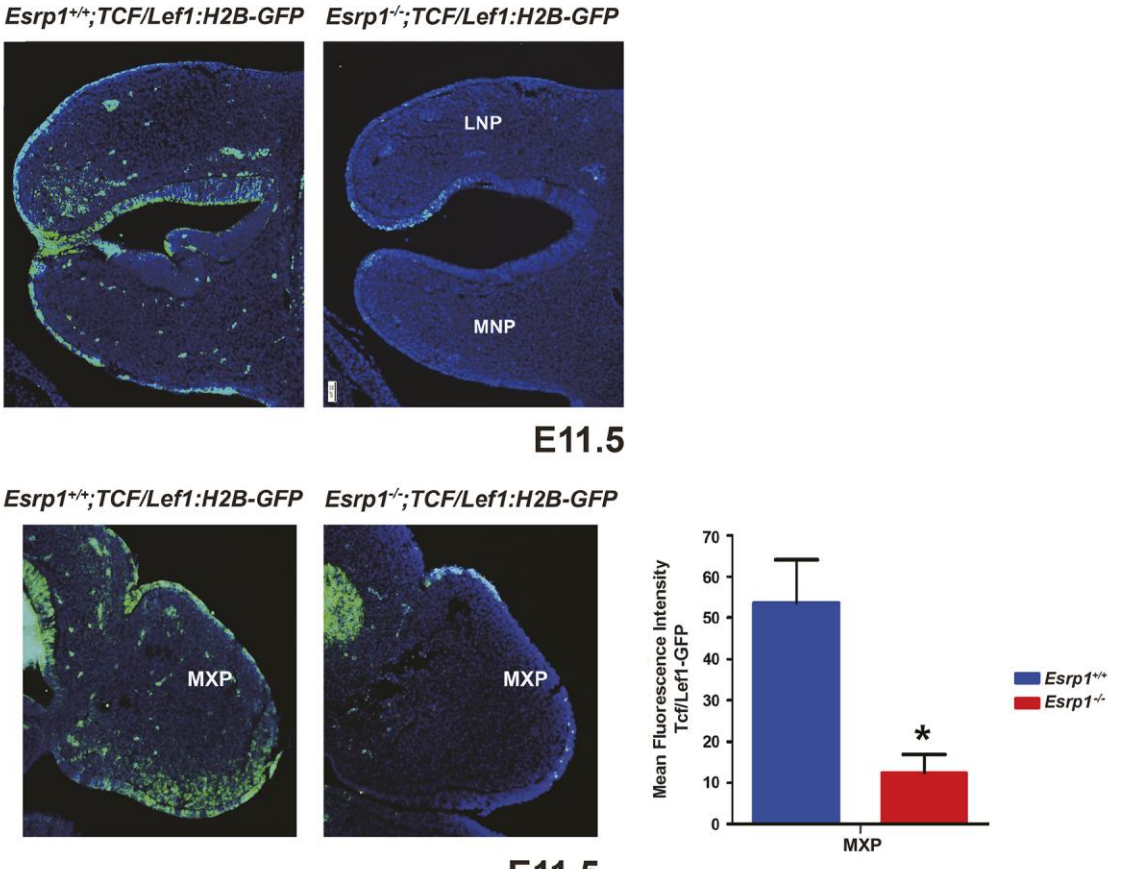

B

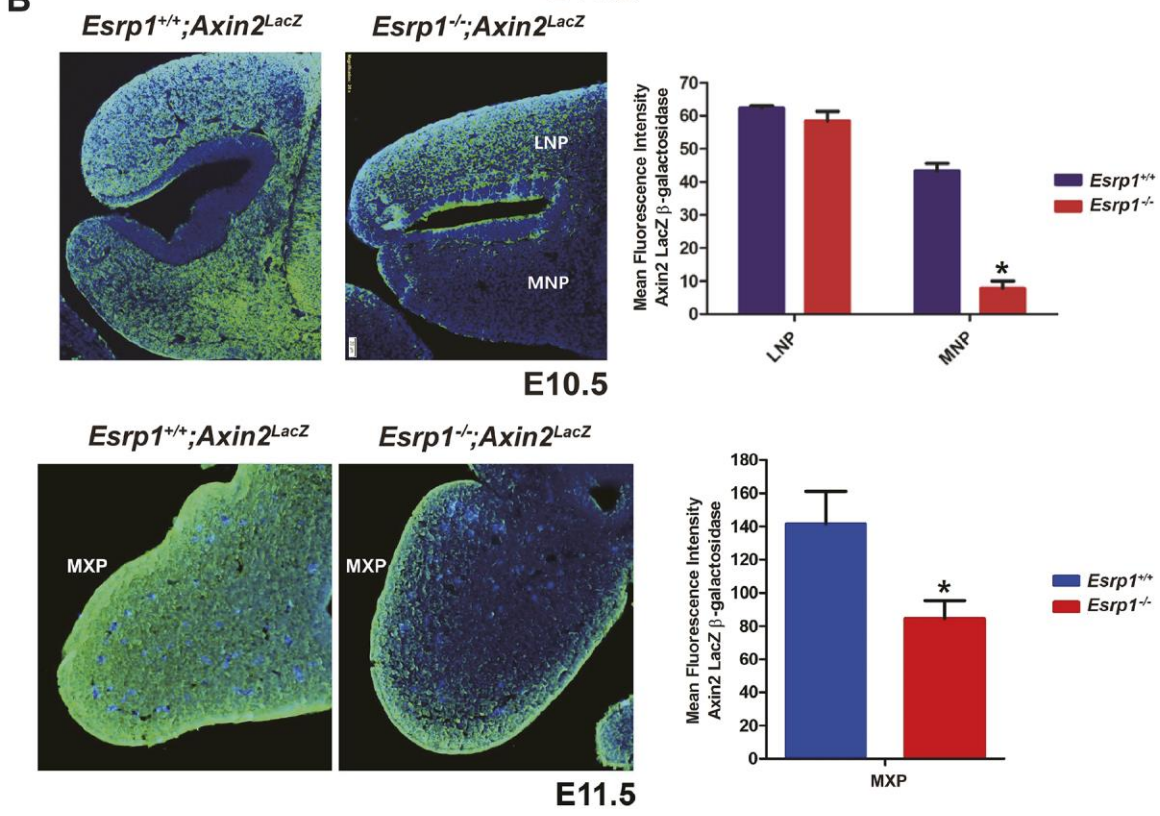

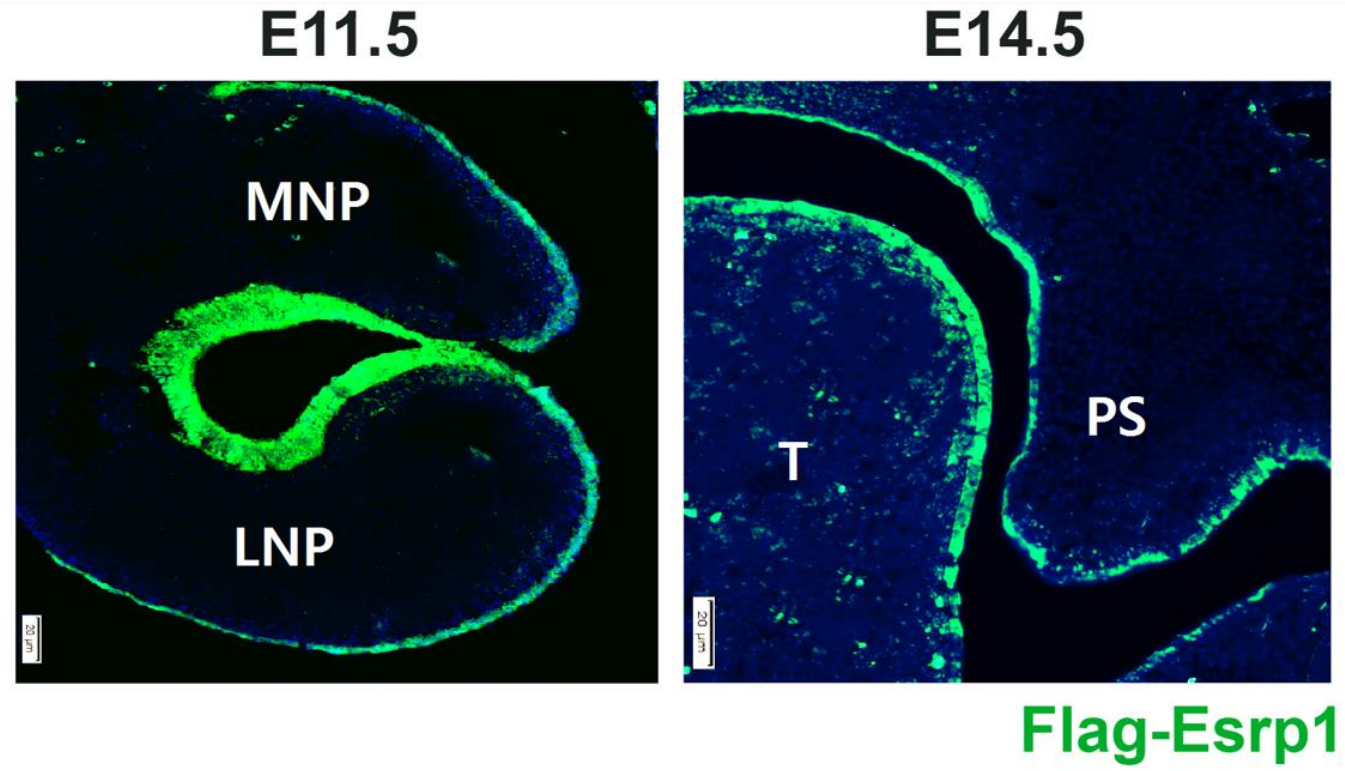

Figure S1. Anti-FLAG immunostaining in lip and palatal sections from Esrp1FLAG/FLAG mice showing epithelial-specific expression in epithelial cells of the developing face and palate.

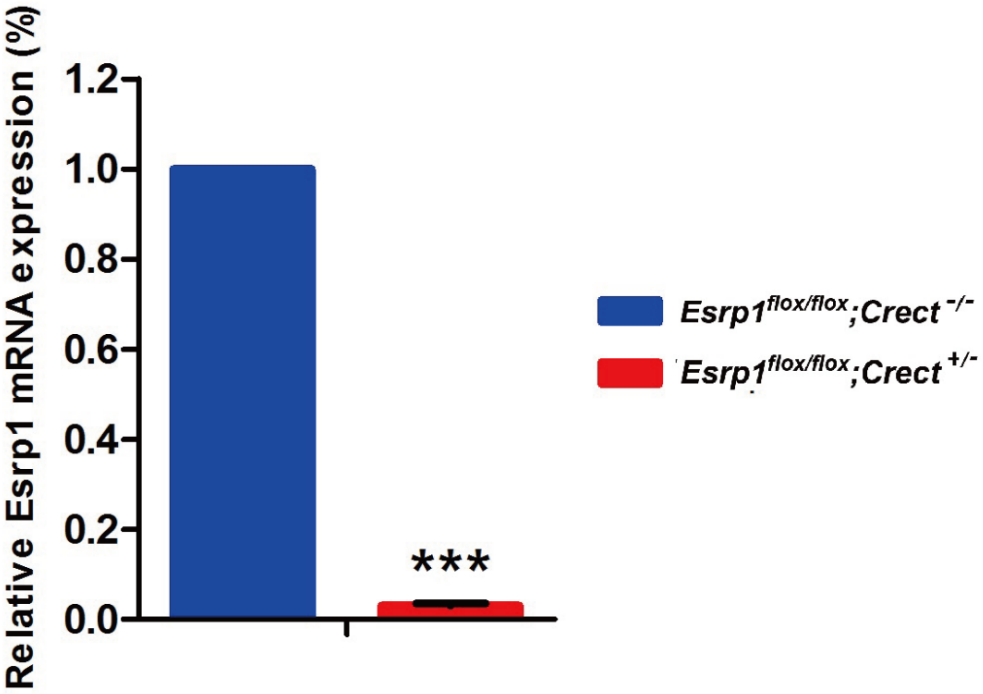

Figure S2. Real time RT-qPCR from E18.5 epidermis from Esrp1flox/flox; Crect+/-embryos showing efficient conditional ablation of Esrp1 compared to WT epidermis.

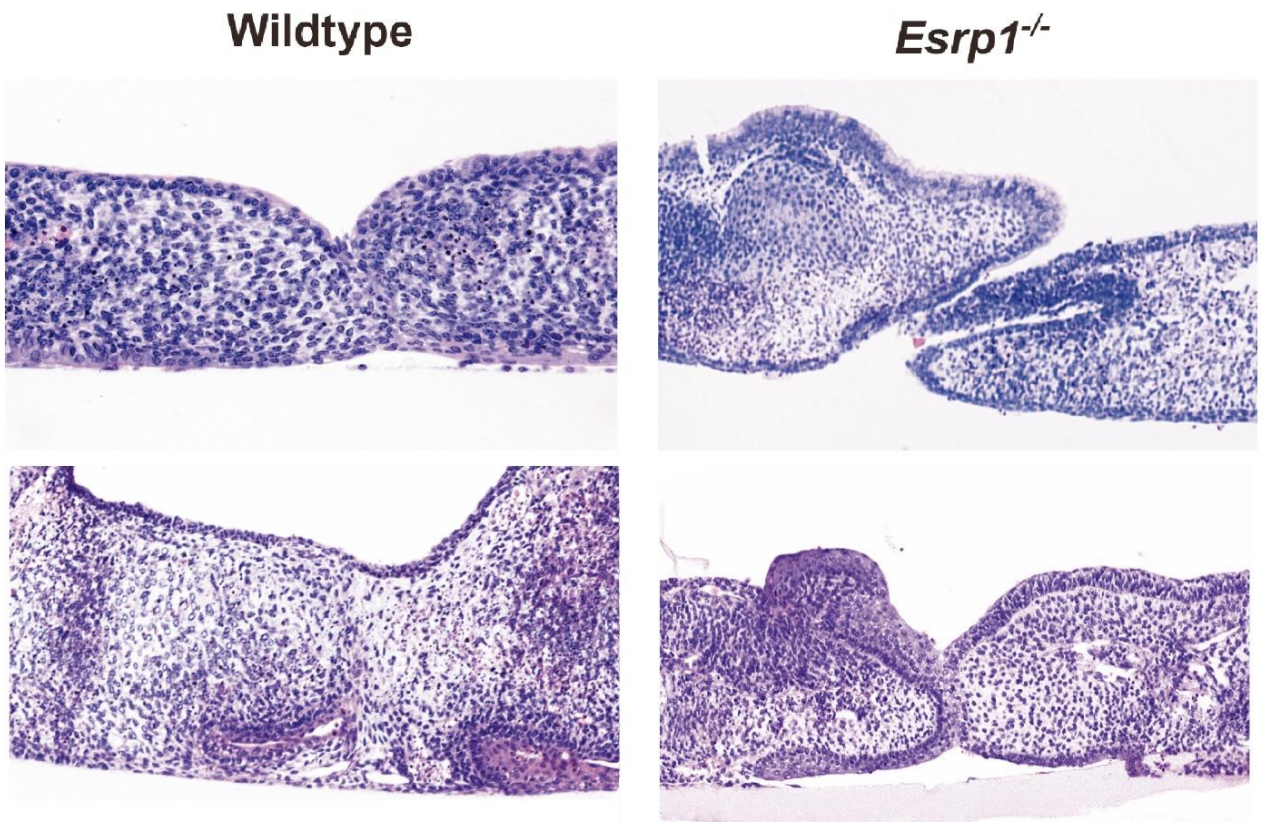

Figure S3. Additional examples of palatal organ cultures showing lack of dissolution of the MES in palatal shelves from Esrp1-/- embryos compared to WT.

Supplemental Tables

Table S1. Complete data file of alternative splicing differences identified by rMATS between wild-type ectoderm and Esrp1 KO ectoderm. Individual tabs represent splicing changes by type. Positive splicing changes were filtered for False Discovery Rate (FDR), 5% and absolute value of predicted change in Percent Spliced In (PSI) greater than or equal to 5%.

Click here to Download Table S1

Table S2. Complete data file of all alternative splicing events identified by rMATS between wild-type ectoderm and wild-type mesenchyme. Tabs and filtering criteria are as indicated in legend to Table S1.

Click here to Download Table S2

Table S3. Complete data file of differences in total gene expression using EdgeR between wild-type ectoderm and Esrp1 KO ectoderm. Events were filtered for FDR < 0.05, and EdgeA>0 (corresponding to CPM (average counts per million) > 1 across all replicates to delete lowly expressed genes. Separate tabs indicate genes upregulated or downregulated in Esrp1 KO compared to wild-type. Another tab contains unfiltered transcript per million (TPM) counts for all replicates.

Click here to Download Table S3

Table S4. Complete data file of differences in total gene expression using EdgeR between wild-type mesenchyme and mesenchyme adjacent to Esrp1 KO ectoderm. The same filtering criteria were used as for Table S3.

Click here to Download Table S4

Table S5. Complete data file of differences in total gene expression using EdgeR between wild-type ectoderm and wild-type mesenchyme. The same filtering criteria were used as in the legend for Table S3 and separate tabs indicate genes that show greater expression in ectoderm or mesenchyme.

Click here to Download Table S5

Table S6. Summary of genes in pathways relevant to CL or CL/P

Click here to Download Table S6

Fig. 6. Reduced Wnt signaling in *Esrp1*$^{-/-}$ confirmed in crosses with WNT/β-catenin signaling reporter mice. Frontal sections (A) Reduced activation of the TCF/Lef1-GFP reporter is observed in ectoderm and mesenchyme of *Esrp1*$^{-/-}$ MNP, LNP, and MXP. (B) Reduced expression of the Axin2-LacZ reporter in LNP and MXP in *Esrp1*$^{-/-}$ embryos. Quantifications are from WT (N=3) and *Esrp1*$^{-/-}$ embryos (N=3). Error bars indicate standard deviation. Statistical significance was determined by two-tailed t-test. *P <0.05. Mean Fluorescence Intensity was corrected for area.

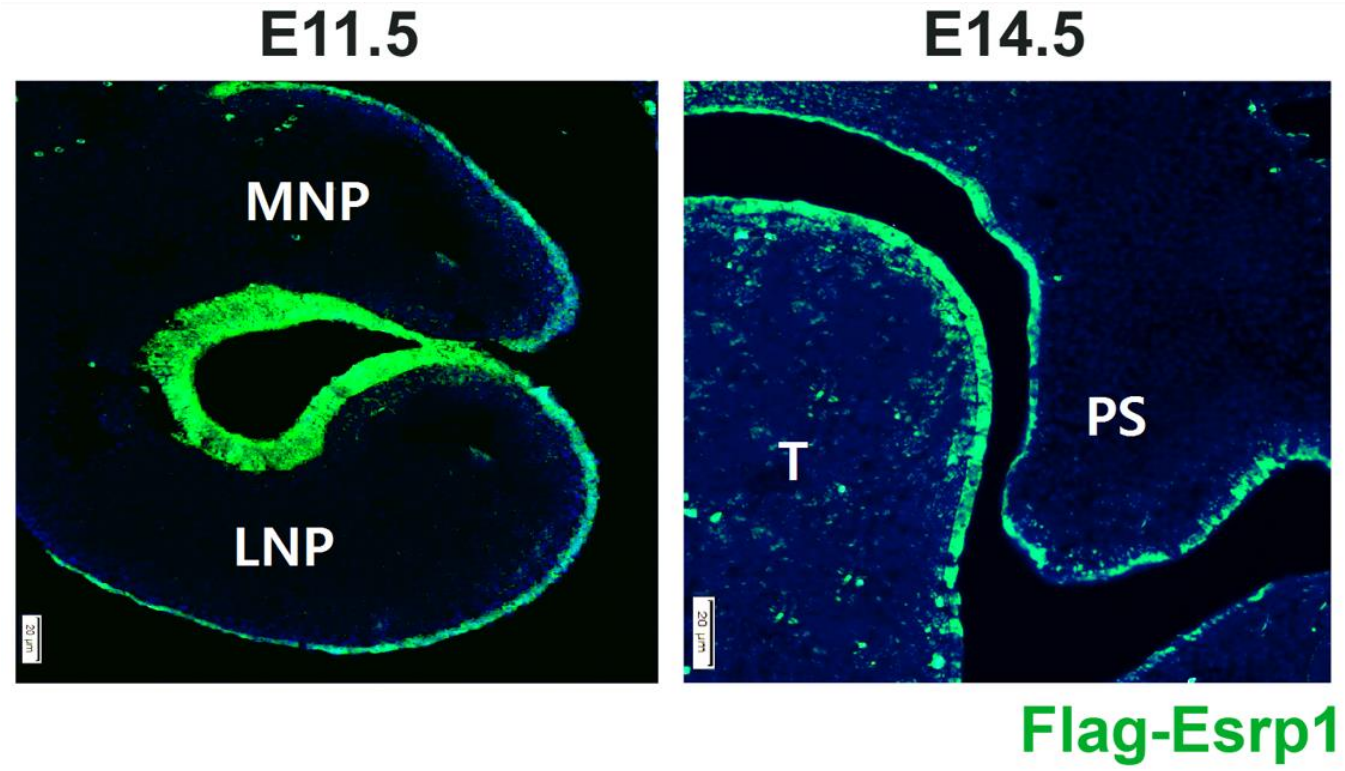

Figure S1. Anti-FLAG immunostaining in lip and palatal sections from Esrp1FLAG/FLAG mice showing epithelial-specific expression in epithelial cells of the developing face and palate.

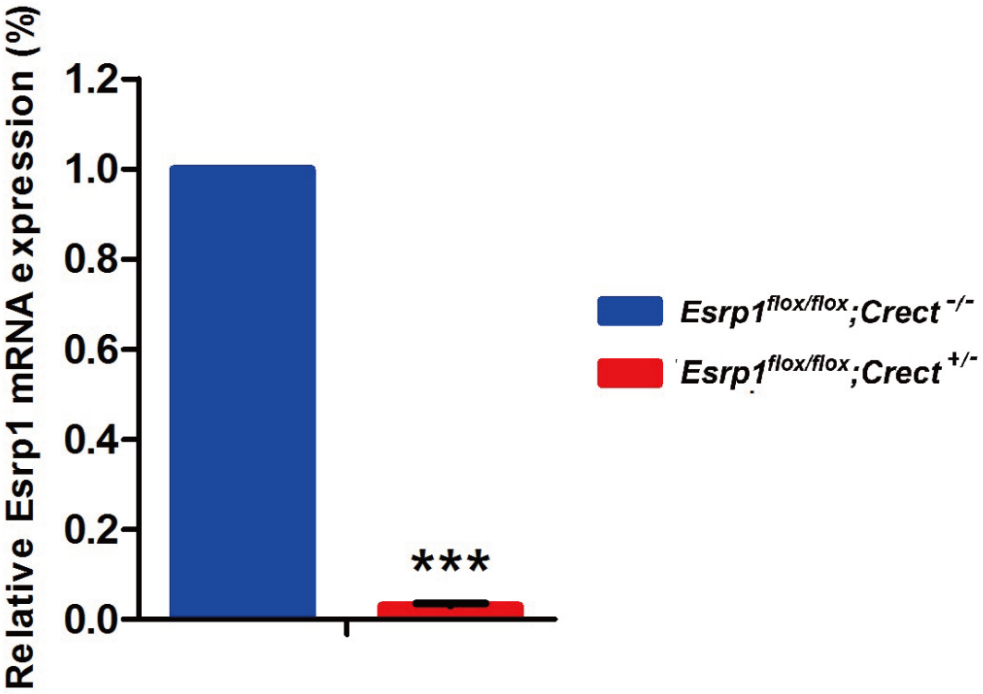

Figure S2. Real time RT-qPCR from E18.5 epidermis from Esrp1flox/flox; Crect+/-embryos showing efficient conditional ablation of Esrp1 compared to WT epidermis.

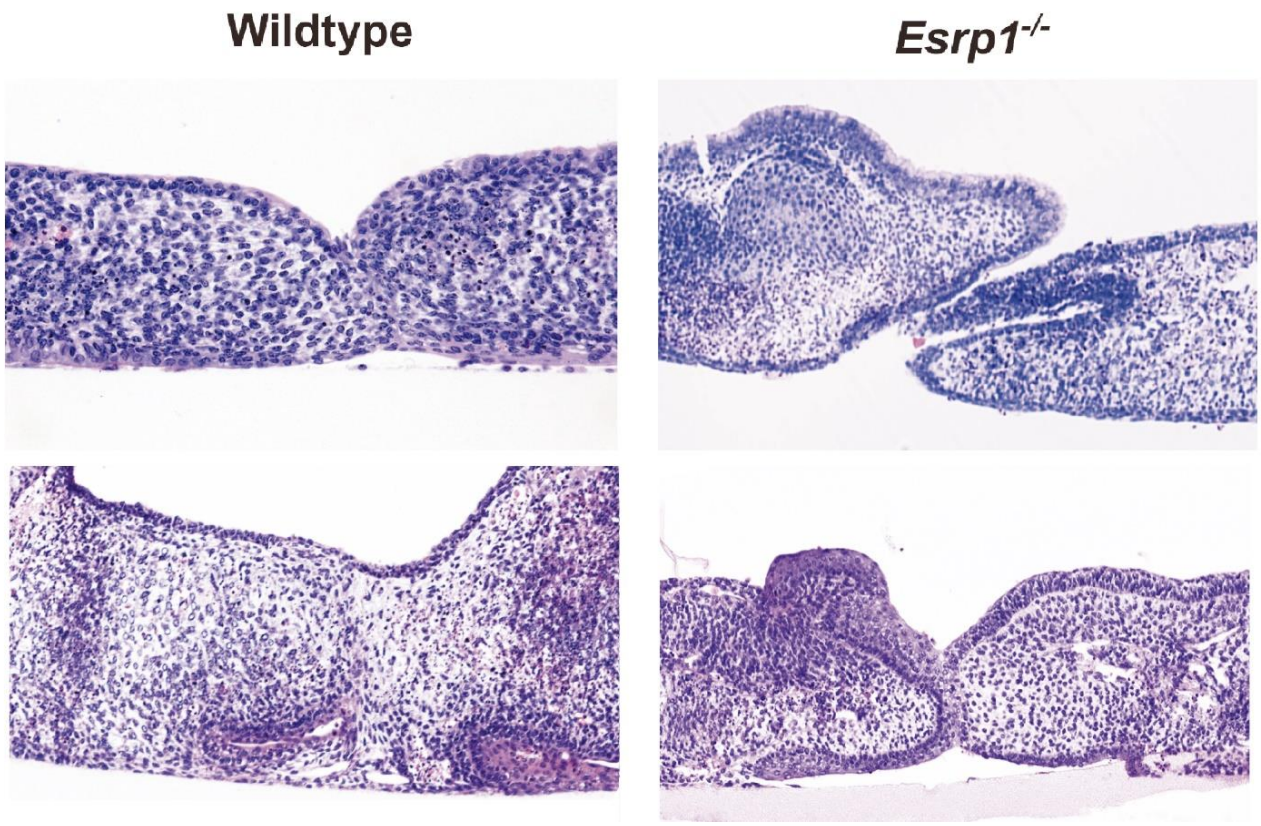

Figure S3. Additional examples of palatal organ cultures showing lack of dissolution of the MES in palatal shelves from Esrp1-/- embryos compared to WT.

Supplemental Tables

Table S1. Complete data file of alternative splicing differences identified by rMATS between wild-type ectoderm and Esrp1 KO ectoderm. Individual tabs represent splicing changes by type. Positive splicing changes were filtered for False Discovery Rate (FDR), 5% and absolute value of predicted change in Percent Spliced In (PSI) greater than or equal to 5%.

Click here to Download Table S1

Table S2. Complete data file of all alternative splicing events identified by rMATS between wild-type ectoderm and wild-type mesenchyme. Tabs and filtering criteria are as indicated in legend to Table S1.

Click here to Download Table S2

Table S3. Complete data file of differences in total gene expression using EdgeR between wild-type ectoderm and Esrp1 KO ectoderm. Events were filtered for FDR < 0.05, and EdgeA>0 (corresponding to CPM (average counts per million) > 1 across all replicates to delete lowly expressed genes. Separate tabs indicate genes upregulated or downregulated in Esrp1 KO compared to wild-type. Another tab contains unfiltered transcript per million (TPM) counts for all replicates.

Click here to Download Table S3

Table S4. Complete data file of differences in total gene expression using EdgeR between wild-type mesenchyme and mesenchyme adjacent to Esrp1 KO ectoderm. The same filtering criteria were used as for Table S3.

Click here to Download Table S4

Table S5. Complete data file of differences in total gene expression using EdgeR between wild-type ectoderm and wild-type mesenchyme. The same filtering criteria were used as in the legend for Table S3 and separate tabs indicate genes that show greater expression in ectoderm or mesenchyme.

Click here to Download Table S5

Table S6. Summary of genes in pathways relevant to CL or CL/P

Click here to Download Table S6

Table S7.

RT-PCR primer sequences used to validate Esrp1 regulated splicing events

Gene	Primer sequence	
Fgfr2	Forward	CCCGGGTCTAGATTTATAGTGATGCCCAGCC
	Reverse	CCCGGGGAATTCACCACCATGCAGGCGATTAA
Ctnnd1	Forward	AACCTCGCTGGATTTGTCTTTC
	Reverse	TGATCCTGGGGTCCGTTGAGTTTC
Enah	Forward	GCTGGGCGTGGGAATGGACCTCTT
	Reverse	TTGCCAGCTCTTTTCTCATCTCAT
Gpr137	Forward	GAAGCGTCGGCCAGAGATGAG
	Reverse	AATGTTGGACCGTCGAGACCG
Flnb	Forward	GGCGAGGAGGTGGGCTTTGTAG
	Reverse	CCTGACGGCAAATGGAATCACCAA
Lef1	Forward	AGCGCGAGACAATTATGGCAAGAA
	Reverse	CCGGGCAAGCTGTGGAGAC
Scrib	Forward	ATCCGCAAAGACACGCCCCACTAC
	Reverse	AGCCTTTTCCCCCTGCGATACTGA
Csnk1d	Forward	CCCAACGCCCCTTACCCCTACCT
	Reverse	GAGCTCCCGGCGTTAACATTTCAG
Mfge8	Forward	ACAGCGTGGGGACATCTTC
	Reverse	TACTATCGTTCGGGACCTA
Arhgef11	Forward	TCAAGCTCAGAACCAGCAGGAAGT
	Reverse	TGCTCGATGGTGTGGAAGATCACA
Arhgef10l	Forward	AGGAGCGCAGGGTCTTC
	Reverse	GATTGTCTTTGTCGTAGGTG
Arhgap17	Forward	ACCCCGAATTCTAATCACTCATCC
	Reverse	GCGGGGGCAGGTTTCTTCACAG
Myo1b	Forward	AAGCGGTACCAGCAGATAAAGAGT
	Reverse	AGTCGAATCCAAGAACAGGTAAGG
Lsm14b	Forward	CCTCGGCGACACAGCTCAATGGT
	Reverse	ATCACAGCTGGGTCCTTCTCTTCC
Plekha1	Forward	CTGATAGCCCTGAAGAGATGC
	Reverse	GCTGCGAGAGGCTGGGGAATGTGA
Epb4.1	Forward	TTAACATCAACGGGCAAGTC

	Reverse	ATATCGGCATCTCCTGTGA
Macf1	Forward	GCAGATAAGATTGAAGATGAGGTC
	Reverse	TATGTTAGTTCTGCCTCGTG
Inpp4a	Forward	GGGGCCCCAGCAGCACAC
	Reverse	TGAGAGCCGTTCCGCGTAGTAGC
Magi1	Forward	AACGCTCCCGCCTGTGAATAGTA
	Reverse	GGCTGAGGCTGCTGCTGTTG
Usp4	Forward	TGAGCCCCAAAATGAAGATG
	Reverse	GAGGCCAGGCTGTATATGAGGTGA

Primer sequences used for real time RT-qPCR

Gene	Primer sequence	
Axin1	Forward	AGAGGTATGTGCAGGCAGTCA
	Reverse	TGTGATTTTGTCTCTGTCTCGGA
Axin2	Forward	TCCAGTCCACCAAACCTATGC
	Reverse	GAAGTCCAGCGTATCCACACA
Wnt3a	Forward	CACCCAACTTCTGCGAACCTA
	Reverse	AGCAGCACCAATGGAAAACAC
Wnt4	Forward	AAGAGGAGACGTGCGAGAAAC
	Reverse	TGTGTCACCACCTTCCCAAAG
Wnt7a	Forward	CAAGGAGAAGCAAGGCCAGTA
	Reverse	GACCCGCCTCGTTATTGTGTA
Wnt9b	Forward	CCCAAGAGAGGAAGCAAGGAC
	Reverse	AACAGGTACGAACAGCACAGG
Fzd1	Forward	ACCAAGGTTTACGGGCTCATG
	Reverse	ACAGCCGGACAGGAAAATGAT
Fzd7	Forward	GTGCTAACGGCCTCATGTACT
	Reverse	GCAACCCGACAGGAAGATGAT
Dvl2	Forward	GTAGGCGAGACGAAGGTGATT
	Reverse	CACCACCCCAAAATCCTGATC
Dvl3	Forward	CTTGGCCTATGGCTTTCCCTTA

	Reverse	AGCTTTTGGGTCCTTCTCCTTG
Tgfb3	Forward	AGTGGCTGTTGAGGAGAGAGT
	Reverse	GTGTGGGTTGTGGTGATCCTT
Bmp7	Forward	GAGGGCTGGTTGGTGTTTGAT
	Reverse	GTTGCTTGTTCTGGGGTCCAT
Shh	Forward	GCGGCAGATATGAAGGGAAGA
	Reverse	CTGCTCCCGTGTTTTCCTCAT
Aldh1a2	Forward	ATGGATGCGTCTGAAAGAGG
	Reverse	TGACTCCCTGCAAATCGATG
Aldh1a3	Forward	AAGAGGGTCACACTGGAGCTA
	Reverse	TCCTCACAAACTCCCCGTAGA
Sfrp2	Forward	AGAATGAGGACGACAACGACA
	Reverse	CCACAGCACGGATTTCTTCAG
Msx1	Forward	AGAAGATGCTCTGGTGAAGGC
	Reverse	GCTCGGCAATAGACAGGTACT
Gli2	Forward	TTCACTTTTCCCCACCCCATC
	Reverse	ACTCGCTGTTCTGCTTGTTCT
Wnt7b	Forward	ACGAGTGTCAGTTTCAGTTCC
	Reverse	AATCGCATAGGTGAAGGCAG
Lef1	Forward	AGCCTGTTTATCCCATCACG
	Reverse	TGTTACAATAGCTGGATGAGGG
Myc	Forward	GCTGTTTGAAGGCTGGATTTC
	Reverse	GATGAAATAGGGCTGTACGGAG
Nfatc1	Forward	TGGGAGATGGAAGCAAAGAC
	Reverse	ATAGAAACTGACTTGGACGGG
Tcf7l1	Forward	CTACAGCAACGACCACTTCTC
	Reverse	GGTAATACGGTGACAGCTCAG
Gapdh	Forward	CTTTGTCAAGCTCATTTCCTGG
	Reverse	TCTTGCTCAGTGTCCTTGC